Energy Consumption Optimization of Powertrain of Electric Underground Load-Haul-Dump Mining Loader

Marius Baranauskas

School of Electrical Engineering

Master's thesis
Espoo 18.2.2019

Supervisor

Prof. Anouar Belahcen

Advisors

Dr. Tatiana Minav
Dr. Olof Calonius

Aalto University
School of Electrical
Engineering

Copyright © 2019 Marius Baranauskas

Aalto University
School of Electrical
Engineering

Aalto University, P.O. BOX 11000, 00076
AALTO
www.aalto.fi
Abstract of master's thesis

Author Marius Baranauskas

Title Energy Consumption Optimization of Powertrain of Electric Underground Load-Haul-Dump Mining Loader

Degree Programme Electrical Engineering and Automation

Major Electrical Power and Energy Engineering **Code of major** ELEC3024

Teacher in charge Prof. Anouar Belahcen

Advisors Dr. Tatiana Minav, Dr. Olof Calonius

Date 18.2.2019 **Number of pages** 59+13 **Language** English

Abstract

The emissions of heavy-duty underground machinery endanger the health of human workers and increase the overall maintenance cost of the underground mine due to ventilation expenses. In addition, tightening emission standards for non-road vehicles are pushing towards greener solutions, hence, fully electric powertrains are becoming a viable alternative for many applications. An electric powertrain is not only local emission-free, but also provides a better controllably and a superior energy efficiency compared to the conventional diesel operated machines. The nature of such vehicles and their periodic duty cycles enable energy optimization and a prospect of an improved efficiency.

The aim of the thesis was to reduce the energy consumption of an underground load-haul dump mining loader. As most of the energy is consumed by the powertrain of the vehicle, the traction motors are the focus of the optimization. An optimal speed profile was generated by means of Bellman's dynamic programming algorithm in MATLAB environment. The simulation utilized dynamic asynchronous motor, battery and vehicle models built according to a real-size experimental prototype. The algorithm had been designed to solve discrete time problems; therefore, the model was discretized with adjustable dynamic accuracy where the intermediate points were obtained by linear interpolation.

The optimal speed profile demonstrated a 9.1% decrease in energy consumption for a generic duty cycle. Additionally, the asynchronous motors were operated at a higher efficiency area generating less heat and in theory prolonging the lifetime of the powertrain components.

Keywords dynamic programming, load-haul-dump mining loader, electric powertrain, energy consumption

Preface

I would like to thank prof. Matti Pietola and the whole Fluid Power team for the research facilities and the economic support.

Otaniemi, 18.2.2019

Marius Baranauskas

Contents

Table of figures

Symbols and abbreviations

Symbols

a	acceleration
a_m	motor acceleration
a_w	wheel acceleration
F_m	force exerted by motor
F_r	rolling resistance
g	acceleration of gravity ≈ 9.81 $[\mathrm{m/s^2}]$
G, g_N	final step cost
H, h_N	intermediate step cost
I	current
I_{m0}	motor inertia
J	cost functional
$\mathcal{J}_N(x^i)$	cost-to-go function at x^i node
k_g	drive gear ratio
k_m	belt drive gear ratio
m	mass
N	normal force
P_{aux}	auxiliary system power
P_b	battery power
P_{be}	maximum battery power
P_m	motor power
r	resistance
r_w	wheel radius
$\mathcal{R}^n$	coordinate space with n dimensions
t	time
T_d	time step
T_w	wheel torque
T_m	motor toque
T_{m0}	motor drag torque
U	voltage
u	control signal
$\mathcal{U}$	control signal u boundaries
v_k	vehicle speed
x	state variable
$\dot{x}$	derivative of state variable x
$\mathcal{X}$	state variable x boundaries
α	slope inclination
η_e	Coulombic efficiency of battery
η_m	motor efficiency
μ_r	rolling coefficient
μ	set of applied controls u
π	control policy
Π	all available control policies π

ϕ_N	penalty function
ω_m	motor speed
ω_w	wheel speed

Abbreviations

BMS	battery management system
CAN	control area network
DAQ	data acquisition
DC/AC	direct/alternating current
DDH	direct driven hydraulics
DP	dynamic programming
ECU	electronic control unit
EMI	electro-magnetic interference
HV	high voltage
LHD	load-haul-dump (mining loader)
NRMM	non-road mobile machinery
STO	safe torque off
VFD	variable frequency drive

1. Introduction

1.1. Background

Underground mines are one of the harshest work environments on the planet. Ensuring the well-being of the mineworkers is one of the major issues for the mining industry. Underground mines, as opposed to open-pit mines, do not possess a natural ventilation, thus proper air conditioning and ventilation systems are essential to combat reduced oxygen levels and elevated temperatures. As the new mines become deeper and hotter, more complex ventilation systems are required. Therefore, the installation and the upkeep of the ventilation systems become a large part of the underground mine maintenance. Despite huge initial investments, the mining history shows that most disasters in underground mines are caused by ventilation system failures – gas outbursts, dust explosions and windblasts (Brake, 2006).

Non-road mobile machinery (NRMM) is the main contributor to the emission levels as most of the NRMM in underground mines are diesel-powered. A fully electric NRMM powertrain is a proposed solution to improve working conditions in the underground mines and to limit the ventilation expenses. The conventional diesel powertrains are a subject of stricter Tier V regulations for non-road engines (Dieselnet, 2016). The tightening emission standards as well as eventual fossil fuel depletion require greener approach to the problem. Even though the conventional powertrains continue to dominate the market (Manzi, 2018), electric powertrains are gaining popularity for both on-road and off-road applications. Electric-powered NRMM is not only emission-free locally but also has a potential to increase work and energy efficiency.

The electric powertrains have numerous advantages over the conventional powertrains. The absence of local emissions provide a safer environment for the machine operators and it reduces the complexity of required ventilation systems. The diesel engine for NRMM applications is usually selected according to the highest load even though the duty cycle is normally composed of short high-power peaks, which results in long idling periods. Electric motors provide great controllability via variable frequency drives (VFD) and have favorable torque-speed characteristics. An electric motor can produce a higher torque when starting form a standstill and at lower speeds. In addition, an inherently lower energy efficiency of an internal combustion engine makes it inferior to the electric motors. Electric motors can be overloaded for almost twice the nominal torque for short amounts of time and they can be operated at higher than nominal speed in the field-weakening region. Therefore, the motor can be downsized, which makes the electric drivetrain more compact than the conventional powertrain. However, the further electric powertrain development is bottlenecked by the energy storage technology. Currently, even the most advanced battery systems cannot compete with liquid fossil fuels in terms of energy density and refueling (recharging) time.

Load-haul-dump (LHD) mining loaders are utilized in 75% of all underground mines to handle loose material during the excavation (Tatiya, 2013). LHD mining loader is type of NRMM, which is similar to a front-end loader but developed for the roughest environments with regard to productivity and safety. However, most LHD vehicles are powered by fossil fuel, which is neither sustainable nor efficient. Electrification and subsequent automatization of underground mines reduce the chance of human-error and introduce an opportunity for

optimization. This thesis analyses a case study of an LHD mining loader and its powertrain energy consumption optimization model.

The next subchapter elaborates on the electric powertrain benefits for underground mine applications.

1.2. Economic, health and environmental factors

Hybrid NRMM are being introduced to the market as an alternative to conventional diesel-only driven machinery (Komatsu, 2018, Innovative Vehicle Institute, 2019). This is an economic based solution, which aims to reduce the maintenance of a LHD loader, while avoiding the use of batteries as the only NRMM power source. Hybrid NRMM is less polluting but does not remove the exhaust factor entirely as the diesel engine is still the main power source of the hybrid powertrain. Despite the local emissions, the hybrid NRMM is more energy and work efficient. Energy consumption simulation published in Lajunen's publication (2010) concluded that the hybrid loader has more than 60% better combined efficiency when comparing to a conventional loader. While 60% is a significant increase from energy point of view, a more significant performance measure for NRMM is tons of material moved per hour (t/h). "*The best work efficiency […] is about 23 percent more than with the conventional loader*" — Lajunen states. This is a noticeable increase in work efficiency, which sparked an interest with new products emerging like "Joy 22HD" hybrid loader (Komatsu, 2018). The manufacturer claims that the work efficiency is increased by 30% and fuel consumption decreases by 20%, which corresponds to the results in the aforementioned article. Nevertheless, the actual work efficiency still heavily depends on the operator of the machine and the percentages have not been validated in an actual work environment.

The fuel cost is only a small portion of the total LHD loader maintenance in an underground mine. Naturally, the newer, deeper underground mines require more complex and expensive ventilation and air-conditioning. To reduce these costs, Tuck (2011) suggests implementing fully electric powertrains. The hourly cost of an electric mining loader taking into account ventilation maintenance is 85 USD/h, which is 30% lower than the diesel powertrain (Jacobs, 2013). The cost sensitivity analysis concluded that the difference is even greater with an increased fleet of mining loaders because more ventilation is needed to retain an acceptable air quality. Furthermore, for every 0.1USD/l increase in diesel fuel price the costs of diesel loaders increase by 2.6 USD/h/unit. The increase in the base cost of electricity actually decreased the costs of electric mining loaders by 4.0 USD/h for every 0.01 USD/kWh increase when comparing to diesel loaders. Overall, running a fully electric underground mine is more economical.

The air quality and the personnel health safety are the major issues in underground hard rock mines (Brake, 2006). Usually in mining applications, NRMM is employed to transport large amounts of ore and other aggregates efficiently. Heavy machinery requires powerful engines to drive them, causing more diesel particulate matter to be exhausted due to incomplete combustion and the impurities of the fuel. There have been major developments in understanding the risks of diesel particulate matter and its linkage to lung cancer and other occupational diseases (IARC, 2012). Understanding and mitigating these risks is the key of

securing the health safety of the mineworkers. As for now, diesel-electric hybrid technology is already being adopted in underground mines due to increased work efficiency and fuel economy. However, hybrid technology is not local emission-free. In that sense, electric powertrains are more attractive than hybrid and other conventional solutions.

Furthermore, a regular LHD mining loader with a conventional internal combustion engine can be as loud as 105dB (Jacobs, 2013). A mining loader equipped with an electric drive operates at only 85dB (100 times less). The noise level of the conventional mining loader is above the limits stated in the Official Journal of the European Union (2003). Therefore, the operators must wear special hearing protection throughout the workday. However, even with the hearing protection, an exposure to high noise levels may lead to an injury or a permanent hearing loss. While short-term effects can disappear after leaving the noisy environment, an occupational illness like tinnitus (ringing in the ears) will weary the regular workers. Hazards like this are taken into consideration while planning the mining works which makes a strong argument in favor of electric powertrains.

1.3. Objectives, scope of the research

The energy efficiency of an electric motor can reach up to 96% for NRMM applications (Havells, 2016). However, this is the case only for a small region in the speed-torque characteristic of the motor. An electric motor never operates at the maximum efficiency during the whole operation – the speed and torque requirements always change. An electric powertrain enables power regeneration during breaking and since the LHD mining loader is a massive machine, there is a great potential to regenerate energy. Naturally, the faster the LHD vehicle moves, the more power is consumed but the harder the vehicle breaks, the more energy can be recovered.

On-road mobile vehicles normally have standard duty cycles, for instance Braunschweig cycle for city busses. Unfortunately, a standard duty cycle for LHD mining loaders are undefined, however, a generic duty cycle is formulated empirically. The automatization of movement according to a generic duty cycle introduces an opportunity for an optimization regarding the energy and work efficiency. Simultaneously increasing work efficiency and energy efficiency is, however, contradictory. While the work efficiency increases, normally, the energy efficiency decreases and vice versa. The proposed optimization method calculates the optimal operation points for the best performance favoring the energy efficiency. A proper work efficiency optimization, on the other hand, could be performed only for a specific case taking into account various economic factors, thus this thesis mainly focuses on energy consumption reduction.

The aim of the research is to reduce the energy consumption of the LHD powertrain traction motors by utilizing an optimization algorithm developed by means of dynamic programming (DP). It is realized by modeling the LHD powertrain in MatLab and applying the optimization algorithm. The optimization code includes a generic work cycle simulation and DP function that minimizes the consumed energy. The simulation generates an optimal speed profile and calculates the total energy consumed and the total time elapsed. The energy consumption results are compared with a profile of constant speed and constant acceleration

(non-optimal velocity profile). By using the simulated optimal speed profile, an approximate operation area is defined and overlaid with the electric motor efficiency map.

This study analyzes the energy consumed by the main LHD powertrain, i.e. the traction motors that are powered by a central battery pack. Other subsystems of LHD, such as work hydraulics and auxiliary systems, are excluded from the simulations or simplified to a constant energy consumption level. In addition, the simulation omits the power consumed by the steering motors for its high efficiency and low power consumption. Thus, the simulation is realized as a movement on a one-dimensional path. The results will be presented in a form of kWh/km (kilowatt-hours per kilometer), which describes the energy efficiency, and time elapsed during the work cycle which corresponds to tons of material moved power hour or work efficiency. This work provides an analysis of an optimization algorithm in an underground mining application. It provides a well-commented MatLab code for the future reference and improvement. Furthermore, it analyses the selection of traction motors, making suggestions for future traction motor improvements for an electric LHD mining loader.

This thesis is organized as follows. Subsection 1.4 contains the state of the art, giving a broader overview of the topic, related research and recent developments. Section 2 defines the laboratory setup of a real-world size LHD mining loader in Aalto University with a detailed specification of the components. Section 3 introduces velocity optimization algorithm, its origins and applicability to this case. Section 4 presents the results of the simulation and discusses the potential application in the mining industry. Section 5 is discussion describing the importance of the findings, probable technical issues and chapter 6 discusses the potential future works and the continuation of the research.

1.4. State of the art

Paraszczak (2014) lists three types of electric powertrains according to the main power source. The drivetrain can be powered by overhead lines or rails, tethered trailing cables or energy storage devices. All three variations are utilized in the industry to some extent. The overhead line method is employed in underground mines that are operated for longer periods because they require higher investment. The high maintenance costs and low adaptability makes it highly unlikely to become the standard solution in the future. Trailing cables is certainly the cheapest solution. However, it is characterized by low mobility and versatility (Lajunen et al., 2016). In addition, the trailing cables introduce an increased chance of failure. The powertrains equipped with a battery pack provide the greatest flexibility and versatility. However, relatively low power capacity of the battery pack limits the operation time of this sort of powertrain. While applications, such as concrete-spray machines with lengthy idling periods, accommodate battery charging, continuous operations of loose material transport require quick charging stations to keep the productivity high. Otherwise, an interchangeable battery pack is necessary. Other alternatives such as hydrogen fuel cells are available but the technology is still in its early development. Overall, despite all the technical challenges, the battery-powered loaders are gaining popularity and more products are expected to emerge in the near future.

The development of a fully electric LHD mining loader is closely related to the battery research. The battery is the weakest part of an electric powertrain when comparing to a conventional powertrain equivalent. Relatively low energy density comparing to liquid fuels, such as diesel or gasoline, and increased chance of battery management system failures are the biggest issues in battery operation and development. Many different battery technologies are being researched but currently, Li-ion technology holds the majority of the market and for good reason. Li-ion has many distinct advantages over other types of batteries, which includes high energy density, low maintenance, availability, and low self-discharge (Buchmann, 2010). Certainly, the technology is not without its drawbacks such as protection systems requirements, aging and transportation issues. Li-ion cells are not as robust as other types of rechargeable batteries like NiCd or NiMH. Li-ion battery packs require complex integrated protection systems to avoid overcharging or discharging the battery cell too rapidly. The battery cells are connected in series to reach the required voltage levels. Furthermore, the voltage of separate battery cells must be balanced during the operation maintaining uniform charging and discharging. Therefore, rigid battery management systems are necessary. The performance of li-ion batteries deteriorate over time, they have limited operation time and the number of charge-discharge cycles. However, Li-ion technology is the most compatible solution for heavy-duty NRMM due to advancing fast and ultra-fast charging systems. The newest technologies can already charge energy capacity of 75kWh in a matter of 5 minutes (Electrek, 2018). That would eliminate the need of a spare battery set, significantly reducing the installation and maintenance costs. Advancements in battery technology directly influences the research of the electric LHD powertrain, making it a more viable alternative in mining applications.

According to Lajunen et al. (2016), NRMM electric powertrains are commercially viable in all power classes. The low power electric vehicles (under 10kW) are the most technologically viable and a variety of products is available on the market. Low power electric NRMM solutions are especially attractive in the environments with low noise and emission requirements. Mid-power class market displays little variety of products. Most NRMM, including LHD mining loaders, utilize hydraulic power transmission for high torque operations such as booms and buckets. The hydraulic power is also used for traction purposes, as the slowly moving machinery currently have no alternatives available, which is one of the incentives for this research. Finally, the high-power class (over 1MW) is exceptionally driven by electromechanical powertrains since the electromechanical transmission outperforms the hydraulic. The relevance of energy efficiency increases as the overheating becomes an issue. LHD mining loaders are considered to be in mid-high power category where the electrification of the powertrain is feasible. Large amounts of energy can be saved because various optimization methods become viable in this power-range.

Dynamic programming (DP) is an optimization technique, based on Bellman-Ford algorithm (1958), which solves the problem backwards in time and stores the relevant information on the optimal trajectory to all intermediate points. It is based on breaking down a complex problem into simple recursive sub-problems. "*An optimal policy has the property that whatever the initial state and initial decision are, the remaining decisions must constitute an optimal policy with regard from the first decision*"- Bellman's Principle of optimality. Dynamic programming is applied in various fields from electrical engineering to logistics and economics. Many algorithms use the concept of dynamic programming including recursive least square method (Hayes, 1996), method of undetermined coefficient (Grimaldi,

2000), word wrapping (Heninger, 2013) and many others. However, the most universal and therefore, most widely used is the original Bellman's algorithm.

Mensing (2013) presents a complex approach to Bellman's optimization problem. The author uses a 3-dimension optimization algorithm (3 state variables) to minimize the energy consumption of road vehicles. However, a 3-dimension DP approach while providing extra accuracy takes substantially more computing power and, consequently, is more time-consuming. One of DP benefits is that it increases the computation time only linearly with the increase of the nodes - the accuracy is cost effective. However, additional input or control signals increase the computation time exponentially. Therefore, a single state – single control method is chosen for this application as was done in Lajunen's (2013) work for electric city buses. The author applied a one-dimensional Bellman's algorithm to minimize the energy consumption of electric and diesel city buses. The method generated energy-optimal velocity profiles for Braunschweig driving cycle (Dieselnet, 2013). The simulation yielded 17% increase in energy efficiency for electric buses and 19% for diesel buses.

Fully electric powertrains are likely to drive the underground mining machinery in the future due to environmental and health concerns. The electric powertrains are more efficient, emit less noise and most importantly exhaust no local toxic emissions. While issues such as battery charging are yet to be solved, the demand for such powertrains are increasing, making it a viable field of research. This study concentrates on the energy and work optimization of an LHD mining loader by means of dynamic programming. A real-size LHD mining loader is analyzed as a platform for this research. The following chapter will describe the laboratory setup in high detail.

2. Description of research platform

2.1. Past projects

A 14-ton LHD mining loader with a 4-ton lifting capacity is available as a case study (figure 1). Currently, the machine is a part of the EL-Zon research project, whose twofold focus is the development of direct driven hydraulics (DDH) and an electrification of NRMM powertrain. A used LHD mining loader was acquired in 2008 for HybLab project in Aalto University. The loader had been operated in an underground mine for 10000 work hours, which is a half of its expected lifetime. Afterwards, the mining loader was taken over by Tubridi project and EL-Zon following that. The goal of these projects were to develop DDH and an electromechanical drivetrain for LHD mining loader.

The original hybrid concept is presented in figure 2. Due to high power of the powertrain, the busbar voltage level was set to 650V. The busbars are protected by a brake chopper and a brake resistor. In case of an overvoltage, the brake chopper sends a signal to the brake resistor and connects positive and negative terminals through brake resistor. The brake resistor dissipates the extra energy in a form of heat, thus a proper cooling system must be installed for a normal application. Diesel-generator (gen-set) and both traction motors are connected in parallel to the main busbars through DC/AC converters. The 362V battery is connected to a choke inductor and a DC/DC converter. The choke is acts as a low-pass filter to protect the battery against sharp voltage surges during the power regeneration period. The DC/DC converter raises the voltage level from 362 to 650V. The steering circuit is also connected to the main busbars, which is protected by charge and discharge circuits and another brake resistor. The steering motors are connected mechanically to drive the steering of the mining loader. More information about the individual components is presented in the next subchapters.

Figure 1: A full-size LHD mining loader in Aalto University laboratory

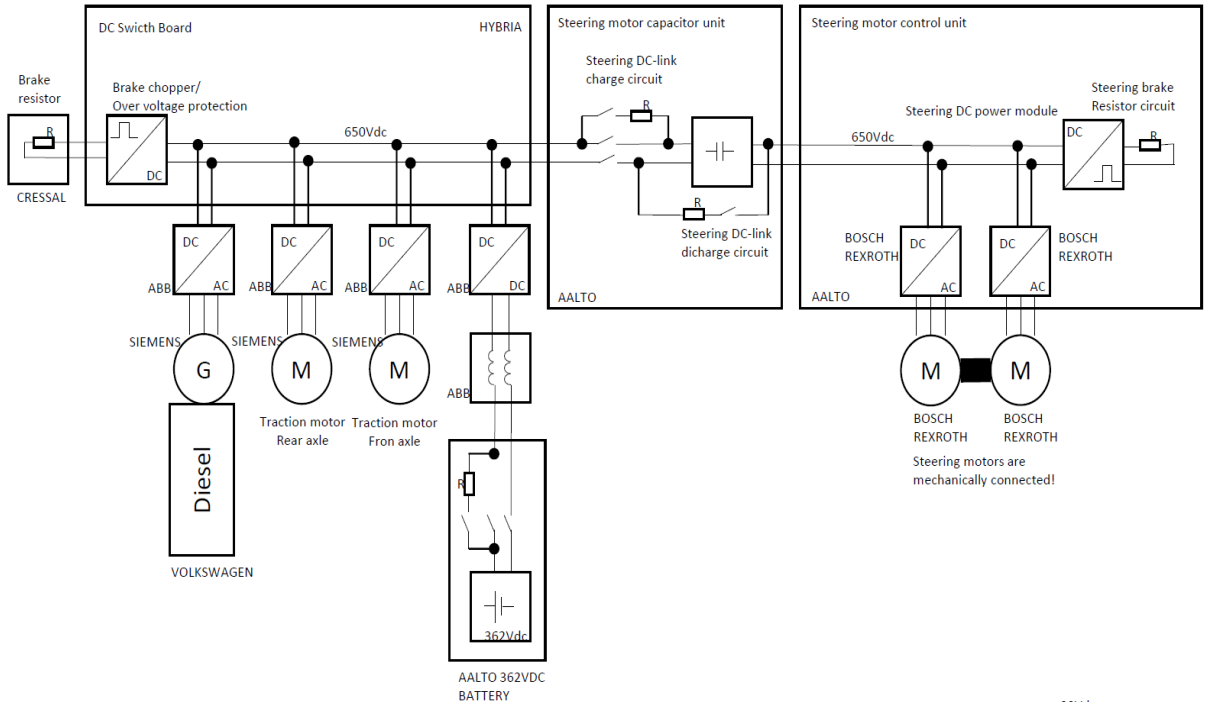

Figure 2: Electric schematic of the parallel hybrid powertrain concept

The following subchapters discusses the separate parts of the LHD mining loader laboratory setup and their role in MatLab modeling and simulations.

2.1.1. Direct Driven Hydraulics

DDH is a hydraulic system that is directly controlled by several electric motors eliminating the need of the central hydraulic circuit. Instead of using valves to regulate the pressure inside the cylinders, electric motors with actuators are used. In recent years, the LHD mining loader had its conventional work hydraulics replaced with DDH. The DDH circuitry and unit components are presented in appendix 1. Numerous articles were published regarding DDH demonstrating its benefits over the conventional hydrostatic hydraulics in terms of energy efficiency and reliability (Minav, et al. 2016 and Lehmuspelto, et al. 2015). DDH as an electrohydraulic actuator combines the benefits of electrical engineering and hydraulics. In a system utilizing DDH, every hydraulic actuator is controlled independently by a dedicated set of pumps driven by electric servomotors. This eliminates the need for a centralized tank used in conventional systems, where all the work hydraulics are connected to a single hydraulic circuit. Therefore, DDH requires less piping and valves, reducing the total volume of the system. It reduces the losses and improves efficiency, eliminating the potential leakage points as well. DDH operates on power-on-demand concept, which means that the DDH drive is only driven when a function is required by a cylinder actuator. This, in turn, reduces the cooling needs and saves energy. The power-on-demand concept is especially beneficial for mining loaders, where the work hydraulics might be used only for a few seconds during the loading/dumping work cycle.

The work hydraulics of the mining loader consists of two main parts: a boom and a bucket. Thus, two separate DDH units were designed and implemented for the loader. Certain constraints were given for the dimensioning of the equipment. First off, the performance of the original setup has to be achieved, this include the speed and the linear force of the boom and bucket functions. In addition, the volumetric dimensions of the original hydraulic cylinders have to be retained. The DDH units are powered by a 96 V battery. A single unit has a motor plus inverter, gear and pump/motors (Lehmuspelto, et al. 2015). The DDH units are identical except for the cylinder part: two double-acting cylinders were used for the boom, whereas only one was used for the bucket.

Comprehensive DDH simulation is not included in MatLab simulation due to its high efficiency and relatively low power consumption comparing to the main powertrain (Turunen, 2018).

2.1.2. Battery

The 362V Li-ion battery (figure 3), designed in Aalto University, consists of 98 cells with 40Ah capacity which is capable of producing 200A. It results in 72kW at a nominal voltage level and 15 kWh of total capacity (Table 1). The battery is equipped with DC fuses, contactors, relays and a pre-charge resistor. The charging is controlled by a battery managements system (BMS). Three hermetically sealed contactors rated at 350A and 750V are the main safety feature of the battery module. The mains DC fuses are rated 400A and 550V, smaller fuses are used to protect BMS (30A) and the test leads for a circuit analyzer (0.44 – 2A). A pre-charge sequence is launched when the battery is connected to an external energy source. The pre-charge resistor has 470 Ω resistance and can handle 500W. The battery is the main power source for traction and steering motors. Inherently it allows recapturing kinetic power during the normal operation and storing it, lowering the overall consumed power.

Figure 3: 362V Li-ion Aalto battery pack

Table 1: Specifications of battery pack

Property	Unit	Cell	Pack
Nominal capacity	Ah	40	40
Nominal voltage	V	3.7	362.6
Max voltage	V	4.2	411.6
Cut-off voltage	V	2.7	264.6
Max charge current	A	80	80
Cont. discharge current	A	200	200
Peak discharge current	A	400	400
Energy	kWh	0.15	14.5

The battery is modelled as the only power source for the powertrain. Figure 4 presents an equivalent circuit of a linear model of the battery. The battery current limits are determined by the maximum charge and discharge currents of the battery cells. Internal resistance is determined by the battery state of charge and the number of battery modules. In case of insufficient battery power, the simulation will use multiple battery packs to provide enough current to drive the powertrain.

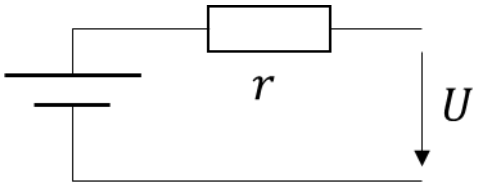

Figure 4: Battery model

2.1.3. Powertrain

During HybLab and Tubridi projects, the original hydraulic powertrain was replaced with a fully electromechanical equivalent. Two traction motors were designed to drive front and rear axles separately, with no mechanical connection in between them. The rear axle is driven by an 85 kW Siemens asynchronous motor with a 1:2 synchronous belt drive and a 3-speed transmission with electromechanical shifting actuators. Rated 3-phase 650V voltage is supplied from a converter module and can provide a rated torque of 220Nm at nominal 142A (530Nm when drawing maximum 300A current) and rated speed 4 000 rpm (max. 10 000 rpm). More information about the motors is provided in Appendix 2. The front axle is driven by a 67kW Siemens asynchronous motor with a belt gear with a 1:3 speed reduction ratio (1:1, 1:2.2, and 1:4.39). For the laboratory setup, the front motor was disconnected mechanically for it is used as a traction assist when the rear wheels are slipping or are in mid-air or when the gear is shifting.

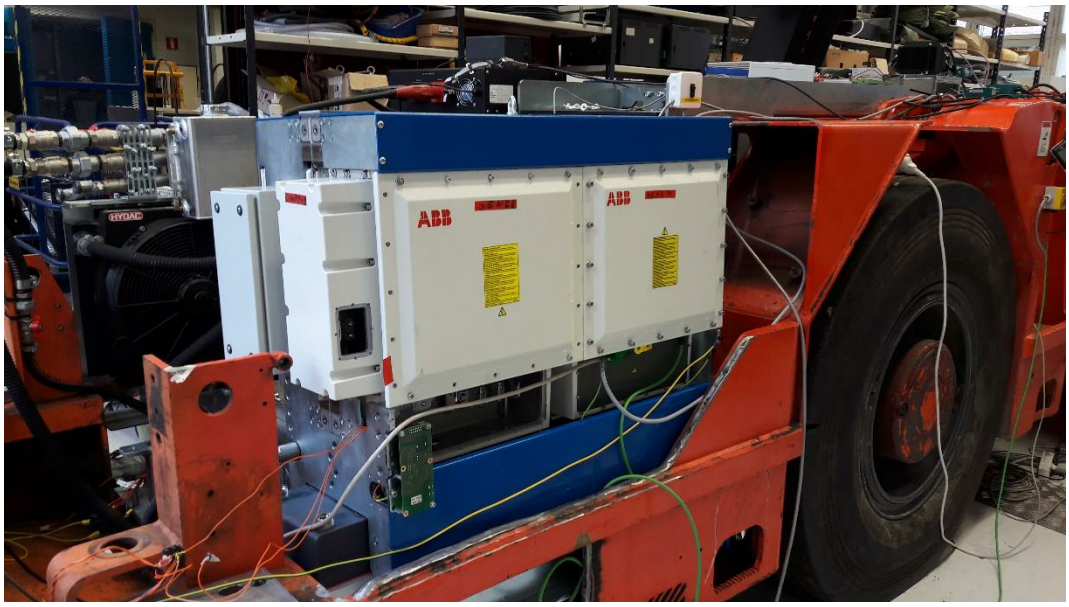

Figure 5: Rack with converters installed onto the mining loader

Table 2: Table of AC/DC converter parameters (ABB, 2018)

ABB Oy	CE		Made in Finland
Type	HES880-104-0320A-5		184KVA IP67
Code	3AUA0000160447	**Serno**	12345678912345
Input		**Output**	
U	700 VDC	**U**	3~...500 VAC
I	N/P 258/388 ADC	**I**	N/P 213/320 AAC
f	DC	**f**	0...1000 HZ
Icc	6KA 1 s	**Date**	14.11.2014

The battery is connected to the motor through ABB HES880 DC/AC converter (table 2). It can support an input voltage up to 700V DC, with nominal and peak DC input currents at 258 and 388A, respectively. Nominal and peak output currents rated at 230 and 320A AC, respectively. Four frequency converters, brake chopper, brake resistor, choke inductor, busbars and other electronics were combined into a rack seen in figure 5.

The mechanical parts of the drivetrain for the front and rear axle are similar, consisting of a belt drive, differential gear and hub gears for the wheels. However, the rear axle has the additional 3-speed gearbox. The drivetrain configuration is demonstrated in figure 6 and CAD drawing in figure 7. The other major difference is the different gear ratios of the belt drives for the rear and the front axle. The gear ratio for the differential gear is same for both axles: 5.125 and the gear ratio of the hub gear is 6.0 for both axles. High gear ratios are beneficial for providing high traction torque for the wheels at high engine speeds.

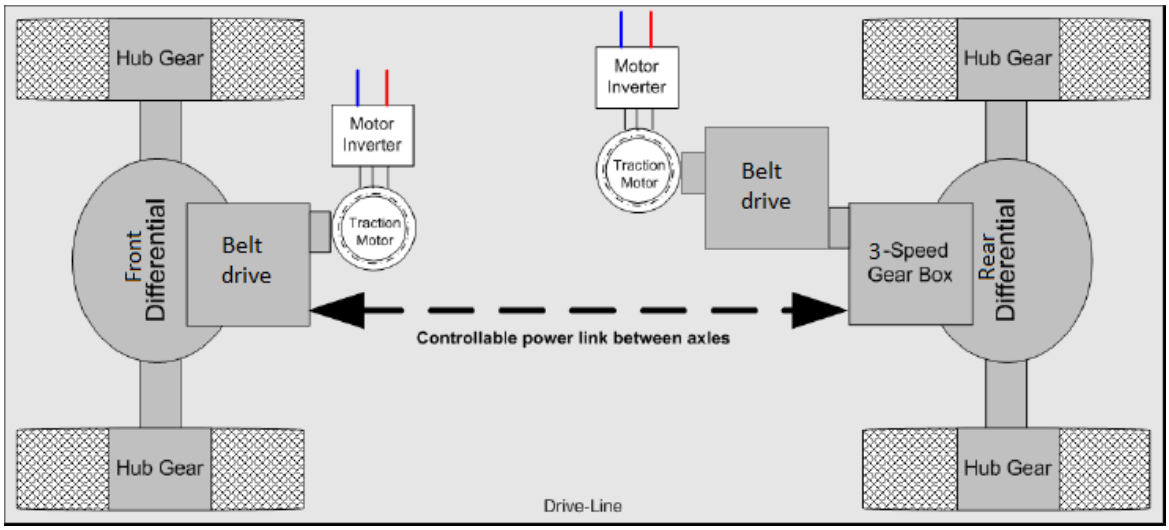

Figure 6: Electromechanical drivetrain configuration. (Liljestrom, 2014)

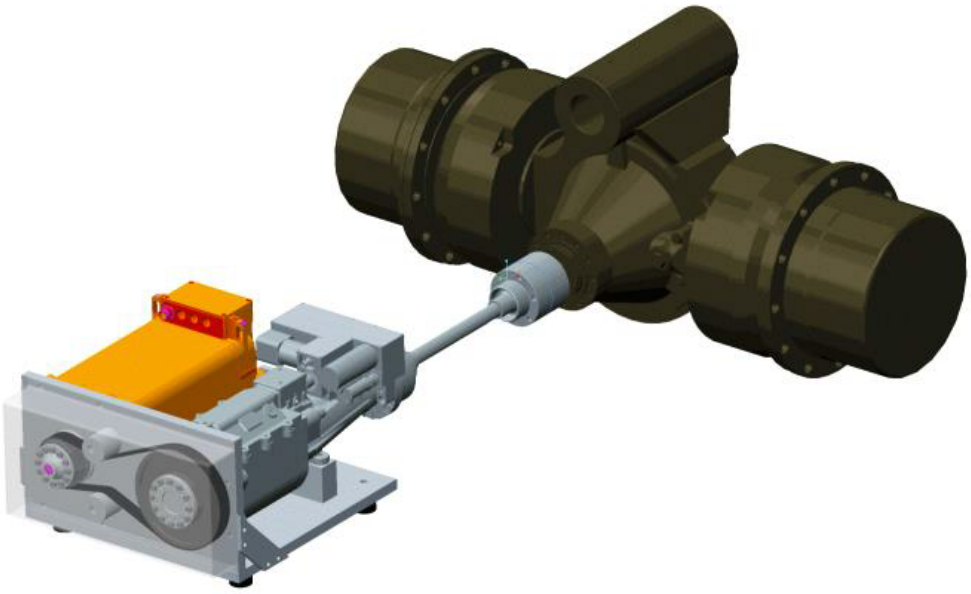

Figure 7: CAD model of rear axle drivetrain, electric motor to wheel hubs (Liljestrom, 2014)

The rear axle motor is equipped with a KT84-130 type temperature sensor, which is a linear semiconductor device with a positive temperature coefficient, i.e. higher the temperature, higher the measured resistance. In addition to the temperature sensor, a 64-tooth wheel speed encoder with two hall sensors is installed. The speed of the motor can be determined from the frequency of the digital I/O signals and the direction of the rotation – from the sequence of the two.

Articulated electromechanical steering is realized by a dual input slew drive with a 1:61 gear ratio, which is installed on the pivot point of the loader. The mechanism has a high efficiency and has no need for a cooling system. Both slew drives (manufactured by Bosch Rexroth) have planetary reduction gears with 1:20 ratio. The drives are interconnected by worm gears

granting a self-locking feature preventing external forces to alter the steering angle. The mining loader has hydraulic parking brakes that are on by default. To relief the brakes pressure needs to be supplied by either a manual pump or an automatic mechanism controlled by a CAN (control area network) bus.

The belt drive features V-shape teeth, which provides a decent grip and requires no lubrication. Although belt drives are not as common in NRMM as in automobiles, it is gaining popularity for its simplicity and ability to dampen shock load. Furthermore, V-belts tend to be the quietest of all the belt drives and much quieter than chain drives.

Since this work does not aim to analyze the mechanical design aspects of LHD loader, only the major components, such as gears, wheels and battery, are simulated the Matlab environment. In addition, several other simplifications are made to make the modelling more reasonable. Due to high efficiency of the steering circuit, it is omitted from the simulation. Therefore, the driving cycle of the LHD loader can be simulated as movement in one dimension. The two traction motors are never loaded equally. The rear axle motor is primary and provides the majority of the load and the other assists when the primary motor is not available. However, that is problematic to simulate, thus the simulation uses two identical equally loaded motors. Finally, the gearbox is not simulated and realized as a constant gear ratio.

Other modelling details are presented in chapter 3. The rest of chapter 2 while not used in simulations but it provides more in depth knowledge about LHD and technical difficulties of such project.

2.1.4. CAN bus

The controller area network (CAN) bus is used in many modern automobile applications. The CAN protocols allow communication between electronic control units (ECU) and sensors without a central computer. It is a robust, low cost, message based control system. Therefore, CAN bus based control was designed for this application as well. The mining loader control schematic has many ECU's (nodes) that would otherwise require complex wiring. Advantages of CAN communication can be defined as follows (CSS electronics, 2018). Nodes communicate over a single CAN interface, providing low cost. The absence of direct analogue signal lines reduces the chance of error, cost and weight. CAN bus allows central error diagnosis and configuration across all nodes – it is a centralized system. The system is more resilient towards EMI (electro-magnetic interference) making it robust enough for mobile applications. CAN messages are ID prioritized, so that the most important messages are not interrupted, contributing to the effectiveness of the system. ECU contains a chip for receiving all transmitted messages and decide their relevance. This flexibility makes it easy to implement new elements, which is especially important for a laboratory setup. The original CAN bus control schematic is presented in figure 8.

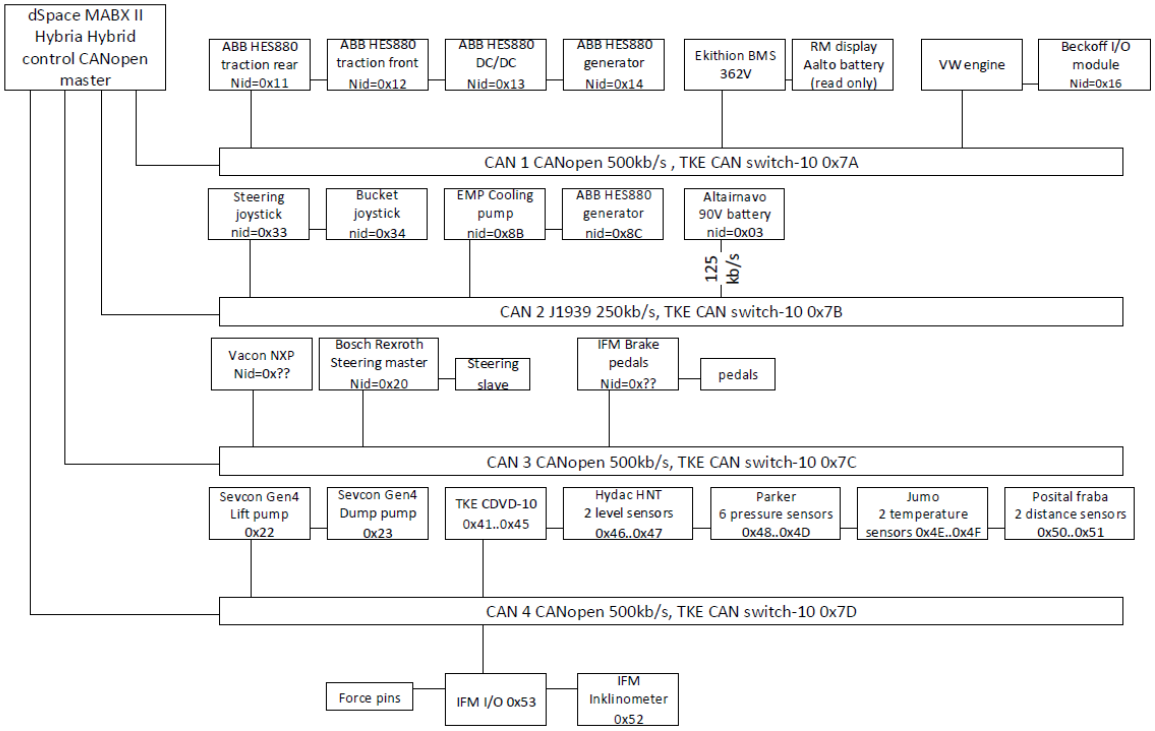

Figure 8: CAN bus control schematic

2.1.5. The parking brakes

The mining loader is equipped with hydraulic parking brakes that are turned on by default. The brakes are spring operated, and hydraulic pressure is needed to relieve them. There are separate brakes for the front and rear axles, but both are connected to the same hydraulic circuit. The parking brakes must be operational for the sake of safety and possible future testing. The brakes can also be relieved by manually pumping oil with a hand pump that is connected to the brake circuit. The pump is connected at the rear end of the mining loader. The pressure required for relieving the brakes is approximately 120-130 bar. Pressures above this range might cause damage to the rear or the front axle, but the system is able to handle pressure peaks up to 180 bar. As no other mechanical brakes are operational, besides breaking by the motor, the parking brakes can be used as an auxiliary breaking system.

The next subchapter concentrates on the present state of EL-Zon project.

2.2. Current state of the project

2.2.1. Electric powertrain

The drivetrain concept was simplified to a fully electric equivalent as seen in figure 9. The front axle motor is not connected to the transmission and only the rear part is operational. The power requirements for the systems were lower than initially planned, thus the busbar voltage was reduced to 362V (the battery voltage). The battery is outdated and its ability to function properly was under a question. Li-Ion battery pack requires a balanced voltage level

across the cells, so the battery charging tests was from regenerative energy was omitted. Therefore, the DC/DC converter and the choke inductor was unnecessary and the battery was connected straight to the busbars. The diesel gen-set (engine and generator) was removed from the setup to make place for the electrical components, as it was not used. DDH and auxiliary (Aux.) component batteries are not connected to the main battery because they are activated separately.

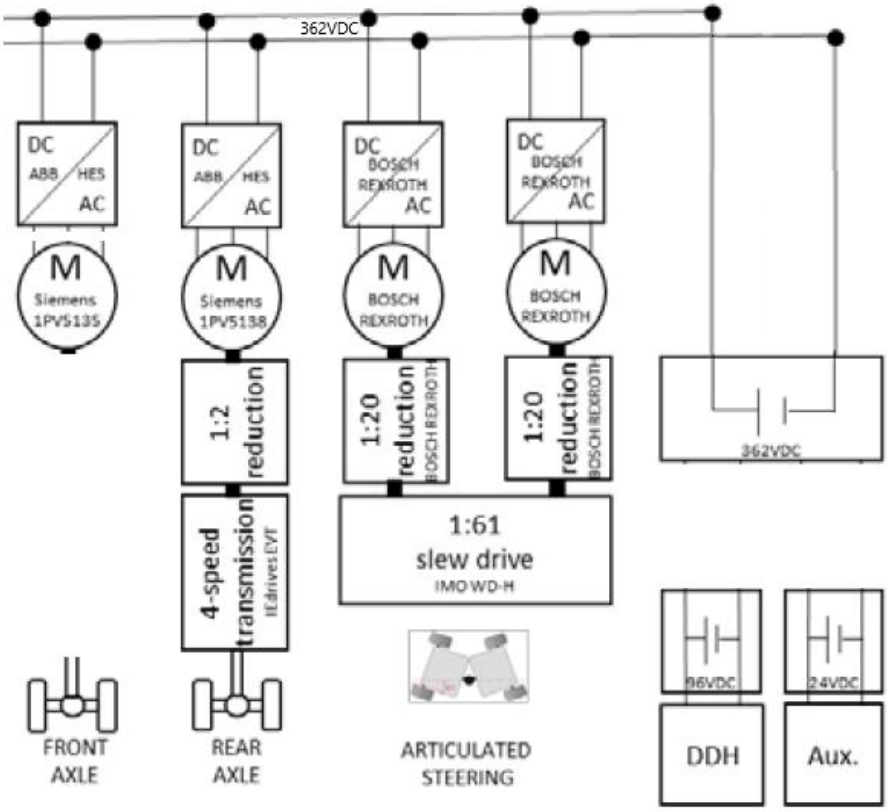

Figure 9: Schematic of a fully electric powertrain

The completed laboratory setup can be seen in figure 10. The maximum current that the motor can draw is around 300A so the cable diameter is at least 70 mm^2. The drive (on the right) can operate in either scalar (speed) or direct torque control (DTC). DTC can provide a very precise control of the torque even without a feedback device i.e. open loop control. The actual feedback is the operator increasing or decreasing the torque reference. To operate in open loop control the drive needs to know how the motor behaves. For that reason, some type of ID run need to be performed. Most ABB drives have different ID run selections: "standstill", "partial" and "normal". "Standstill" is the only one possible if the motor cannot be disconnected from the load. This method will only magnetize the motor and will not necessarily provide the best results. "Partial" torque ID run will cause the motor to rotate slightly but it will not reach the rated speed and torque. The preferred type of ID run for most applications is "Normal". The motor has to be disconnected for this type of test. First, the motor is at standstill while the drive is calculating the required magnetizing current, which is an equivalent of a standstill ID run. Afterwards, the motor is accelerated to the full speed in the forward direction, then given several different speed settings and torque pulses.

“Normal” ID run was performed on the mining loader motor, as the transmission was disconnected from the wheels. The motor ID run requires entering the motor parameters. The traction motor parameters as seen by VFD is shown in table 3.

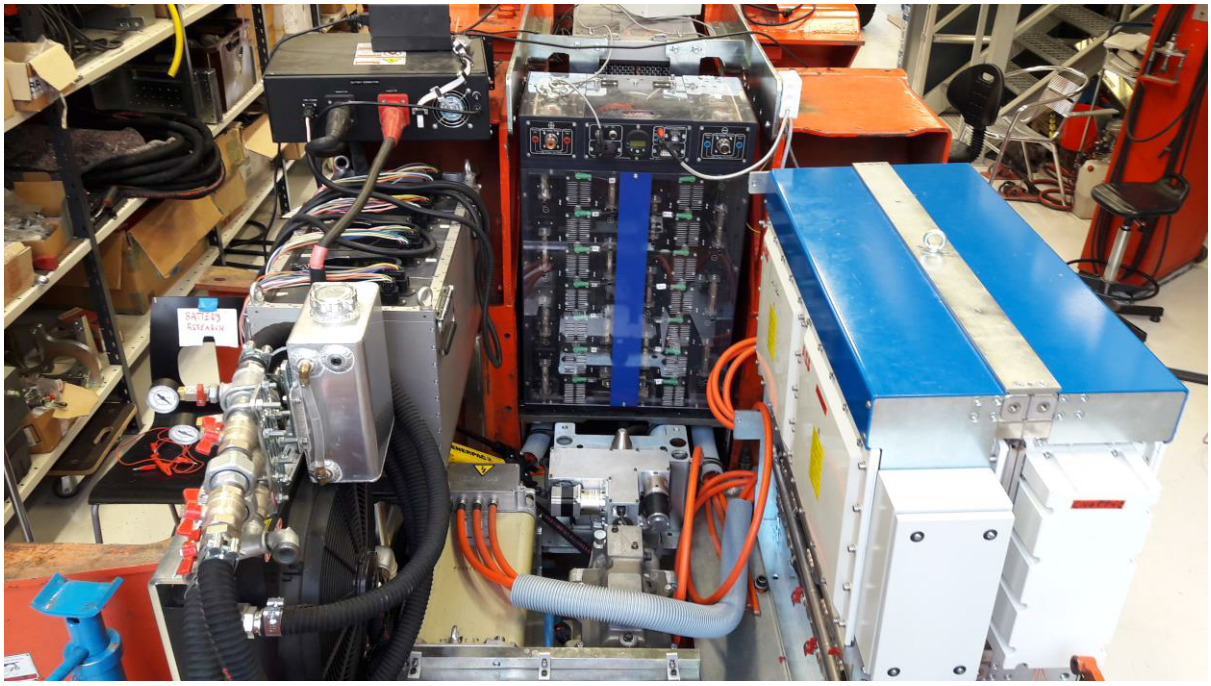

Figure 10: Laboratory setup of an electric powertrain

Table 3: Traction motor parameters as seen by VFD

	Value	**Unit**
Motor type	Asynchronous motor	-
Control mode	DTC	-
Nominal voltage	440	V
Nominal frequency	133,7	Hz
Nominal speed	3920	rpm
Nominal power	85	kW
Nominal $cos\phi$	0,87	-
Polepairs	2	-

2.2.2. The cooling system

The cooling system is designed for the DDH units and the electric components placed in the rack and the traction motor. The main unit consists of two centrifugal pumps: one for the DDH units and one for the electric components. The main unit is also equipped with a fan and a radiator for cooling the circulating liquid. All of the cooling equipment is operated is powered by 24 V, together with other auxiliary systems. The presence of a cooling agent in the system is necessary for laboratory testing conditions because a similar traction motor had been overheated in the past. Since the main electric circuit was modified, a cooling circuit could also be simplified. The main unit, the converter, the rear traction motor were connected in series. In addition, two pressure sensors were installed for the main unit: one for monitoring the outlet pressure and the other for monitoring the pressure on the inlet. The pressure sensors were used to confirm that the system pressure would not exceed 2.5 bar, which is the maximum pressure for the motor; the maximum allowed pressure for the inverter is higher. The system was filled up with water after the physical connections had been made. The volume for the entire system was approximately 12 l. The Siemens motor manual recommends using a 50/50 water-glycol mixture. However, only water was used to test for any leakages. Water-glycol mixture is added later for an extended operation time. This simple cooling system together with temperature sensors protects the traction motor and other equipment from overheating.

2.2.3. Analog control joysticks

While CAN bus is used frequently in automobile industry it not without disadvantages: it is difficult to debug and it is not always reliable. CAN bus control was a logical selection for the original hybrid powertrain because many ECU's need controlling. However, for a fully electric drivetrain CAN bus is an overkill. The control of one traction motor and two DDH units were realized as an analog control. The CAN joysticks were rewired to function as analog controller (similar to potentiometer). Two joysticks were used: one was to control the speed on the motor and the other for the hydraulics of the bucket and the boom. The joystick has 2-axis control and a trigger button. The control was designed to be intuitive from the driver's point of view. One axis is used to control the speed of the motor, the trigger acts as a safety feature (the motor runs if the button is pressed) and the other axis is left for a steering control. The joysticks are places in their original positions at the driver's seat.

Figure 11: Installed joysticks

The actual validation can only be possible in the natural work environment i.e. an underground mine. However, this chapter described the research platform for this thesis. Thus, a MatLab model was developed based on the aforementioned case study of a completed LHD mining loader. An optimization algorithm was applied for the model and the duty work cycle. The model, the duty work cycle and the speed optimization algorithm are described in detail in chapter 3.

3. Speed optimization method

A control system is designed either by a trial-and-error process (tuning the parameters manually) or by an optimization algorithm. While trial-and-error method does not require profound control engineering skills, it can be very time consuming and the parameters determined will not result in the best possible performance. The objective of the optimal control is to determine the control signals which cause the process to minimize (or maximize) some performance criterion at the same time satisfying the physical constraints. Optimizing the work cycle of a mining loader is beneficial because it normally operates at periodic duty cycles over its lifetime. The operation is highly energy consuming, so even a small increase in energy efficiency, will result in many kWh saved. The speed control of the mining loader is the subject of this study, which is formulated as an optimization problem.

The optimization method for this study is based on Dynamic Programing and Optimal Control textbook (Bertsekas, 2005). The objective of the optimization is to minimize a certain cost or mathematical expression of an undesirable outcome. The DP technique captures a desire for a low present cost and a high future cost tradeoff. It is achieved by ranking the decisions based on present cost and the expected future cost assuming the optimal decision making (control policy) for the subsequent stages. DP can be utilized for a broad variety of problems irrespective to the structure of the problem. An acceptable model for an electric powertrain optimization is a dynamic system with a finite number of stages (finite horizon). The model features a discrete time dynamic system, a cost function that is additive over time and no stochastic input.

The DP technique relies on the principle of optimality, which suggests that an optimal control policy can be constructed in piecewise fashion. It starts from the end of the problem and calculates an optimal policy for the last segment sub-problem then extends the optimal policy for the last two-segment sub-problem and continues in this manner until it constructs an optimal control policy for an entire problem. The following subsection presents a mathematical expression of a basic DP problem. The basic problem is very general and does not require that the state or control parameters have finite values or belong to n-dimensional vectors.

3.1. General mathematical expression of Bellman's algorithm

The general idea behind DP is breaking down the problem into sub-problems, solving them and reusing the solutions. The DP is a powerful tool for many applications such as finding the shortest path, calculating a minimal cost of an industrial process or even solving hybrid-energy management problems (Back, et at. 2004). It is occasionally called a "careful brute force algorithm" because it involves an exhaustive search in polynomial time. However, it solves the optimization problem backwards in time omitting the redundant operations of a basic recursion algorithm. This is especially important for the problems with many nodes (variables) because it saves relatively more computation time. According to Demain, MIT (2011), the DP is utilized by following these four steps. First, the problem is classified as a dynamic programming problem and sub-problems are created with a possibility for recurrence. Second, a state variable is decided. Third, the relation between the states is formulated, and finally, memoisation is added. Therefore, even if the problem does not

inherently deal with an optimization, it can be reformulated and used with a DP algorithm, making it a very powerful and universal tool. Below is a general mathematical expression for a DP algorithm.

The class of optimal-control problems, which can be solved using DP, is written in state space equations [1]-[5]

$$x(t) \in \mathcal{X}(t) \quad [1]$$

$$u(t) \in \mathcal{U}(t) \quad [2]$$

The optimal-control problem in question is time-variant, thus, both the state $x(t)$ and the control $u(t)$ depend on time t and they are defined within the sets of $\mathcal{X}(t)$ and $\mathcal{U}(t)$ respectively.

$$\dot{x}(t) = F(x(t), u(t), t) \quad [3]$$

where $\dot{x}(t)$ is a derivative of state space $x(t)$ and it is a function of the state space, the control signal and time.

$$x(0) = x_0 \quad [4]$$

$$x(t_f) \in [x_{f,min}, x_{f,max}] \quad [5]$$

The equation [4] defines the initial value of the state space and the equation [5] sets the final state constraints.

The DP optimization goal is to minimize (or maximize) some criterion $J(u(t))$ by applying the control $u(t)$, i.e:

$$find \min_{u(t)} J(u(t)) \quad [6]$$

which is also known as the cost functional. It is generally defined as follows

$$J(u(t)) = G\left(x(t_f)\right) + \int_0^{t_f} H(x(t), u(t), t)dt \quad [7]$$

where $G\left(x(t_f)\right)$ is the final step cost and $H(x(t), u(t), t)$ is the cost of an intermediate step.

To utilize DP MatLab function, the continuous time problem is discretized, thus, the state variable is

$$x_{k+1} = F(x_k, u_k), \quad k = 0,1, \dots, N-1 \quad [8]$$

where N is the total number of nodes. Subscript k and lowercase letters (g and h) are used to indicate the discrete domain.

Let the control policy π be a set of all applied controls u_k:

$$\pi = \{u_0, u_1, \dots, u_{N-1}\} \quad [9]$$

Then eq. [7] is discretized with the initial state

$$J_\pi(x_0) = g_N(x_N) + \phi_N(x_N) + \sum_{k=0}^{N-1} h_k\big(x_k, u_k(x_k)\big) + \phi_k(x_k) \quad [10]$$

where g_N represents the final cost in [7] and ϕ_N is an additional penalty function which is used to enforce the constraints of the final state [5]. h_k is the cost for applying the control u_k at x_k and the state constraints [1] are enforced by ϕ_k.

The optimal policy π^0 is the one that minimizes the J_π.

$$J^0(x_0) = \min_{\pi \in \Pi} J_\pi(x_0) \quad [11]$$

where Π is all the available control policies.

Based on the principle of optimality, cost-to-go function $\mathcal{J}_k(x^i)$ is evaluated at every node backwards in time in the discretized state. Thus the cost-to-go for the final step is

$$\mathcal{J}_N(x^i) = g_N(x^i) + \phi_N(x^i) \quad [12]$$

and the cost-to-go of any intermediate step:

$$\mathcal{J}_N(x^i) = \min_{u_k \in \mathcal{U}_k} \left\{ h_k(x^i, u_k) + \phi_k(x^i) + \mathcal{J}_{k+1}\left(F_k(x^i, u_k)\right) \right\} \quad [13]$$

The optimal control is defined by the argument u_k that minimizes the right-hand size of equation [13] for each x^i at the time index k. $\mathcal{J}_{k+1}$ is evaluated on discretized points in the state space and other points are determined by linear interpolation method. The output of the algorithm is an optimal control signal map, which is then used to find the optimal control signal during a forward simulation. In contrast to "brute-force" optimization methods, increasing the number of nodes (accuracy) increases the simulation time linearly and not exponentially. However, the complexity of the DP algorithm is exponential with respect to the number of state and input variables. In this case, only one state and one input variable are used, therefore the simulation time is relatively low. The following subchapter delves into the specifics of MatLab function that is used for the modelling.

3.2. DPM function

This research was inspired by the results published in Lajunen's (2013) work. The article claims 17-19% energy consumption decrease for electric buses using a DP optimization method. The electric bus and NRMM powertrains share certain similarities, thus a similar optimization outcome can be expected. However, the electric bus was optimized for a rather complex Braunschweig cycle, composed of many sub-cycles with rapid acceleration and deceleration periods. The NRMM duty cycles, on the other hand, are either undefined or rather simple, reducing the capacity for the optimization. The backbone Lajunen's work and this thesis is a DPM optimization function developed by O.Sundstrom and L.Guzzella (2009). The DPM function is developed according to DP Bellman's algorithm described in the previous subchapter. The DPM enabled a broader use and easier approach to for DP optimization algorithm. Figure 12 presents a flowchart of the algorithm.

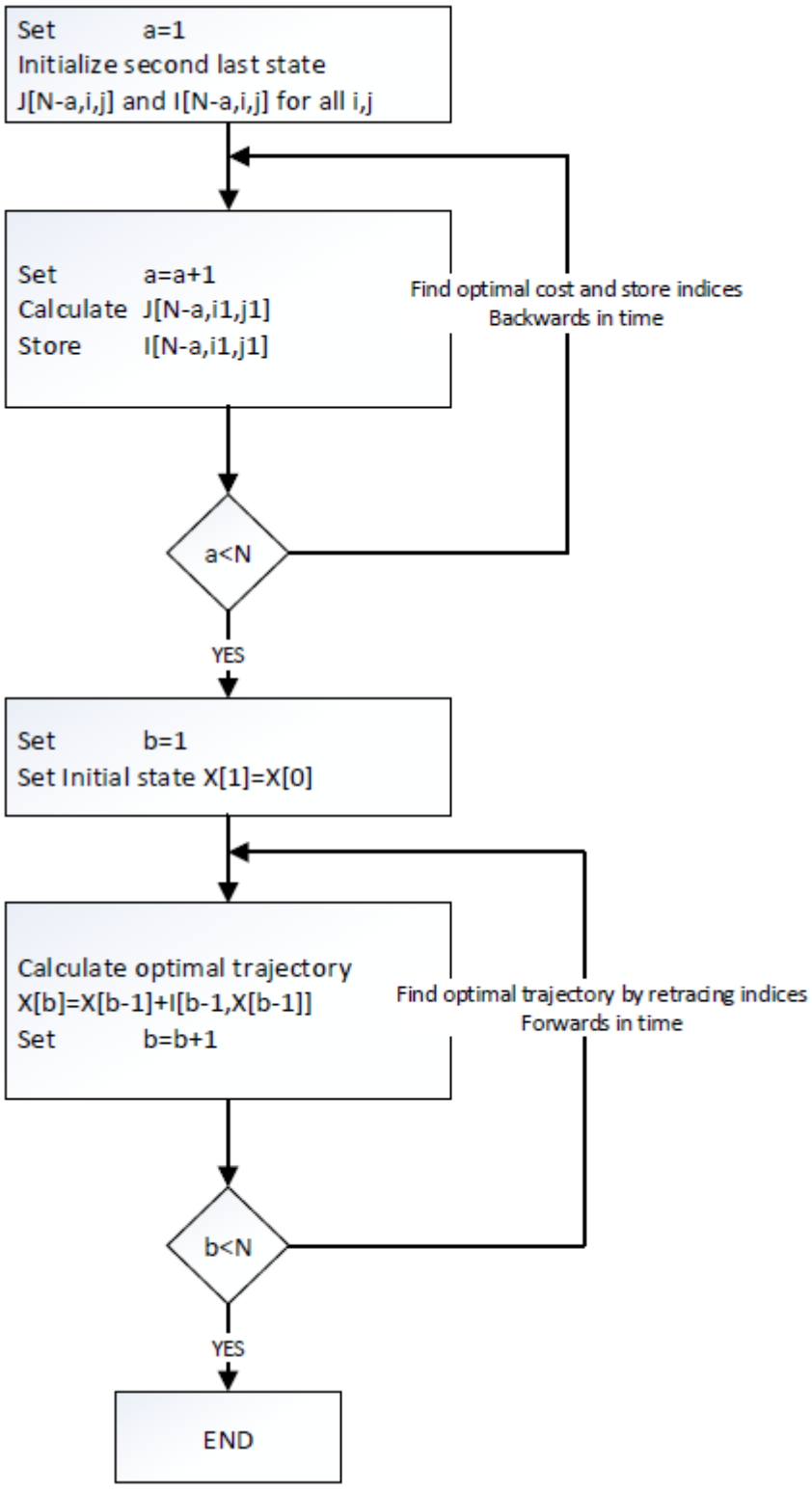

Figure 12: DPM flowchart

The algorithm consists mainly of two parts – searching for the optimal path backwards in time by storing the indices and finding the optimal trajectory by retracing those indices

forwards in time. The simulation backwards in time solves the problem from the end (a certain position and speed by the end of the duty cycle) and finds the optimal control policy for the second last state. The algorithm then saves the indices corresponding to the optimal control policy for the "tail problem" and keeps adding nodes until it reaches the initial state. For lengthy problems, the first loop is considerably more time consuming because the algorithm calculates all the cost functions for the every possible control policy.

As mentioned before, the DPM function is a universal tool with a predefined structure. The function requires five inputs - FUN, PAR, GRD, PRB, OPTIONS. FUN is a function handle with a model description, which is described in the following subsections. PAR contains the user defined problem parameters, including the time step, length of the problem, start time index and a possible disturbance input (unused in this model). The function assumes equally spaced grids and GRD defines the structure of the problem. It defines the initial state, number of elements in the state and input grids (the accuracy of the simulation), state and input grid boundaries (in this case, the minimum and maximum speed and position of the vehicle), upper and lower final state constraints (the position of the vehicle by the end of the duty cycle). According to the author, the DPM function works well for grid sizes with fewer than 5 000 000 points. OPTIONS provides additional customization for the simulation such as toggle waitbars and warnings, select discrete or continuous input, boundary method and other.

The DPM function is an open source and it available online. It includes over 2400 lines of code and is available online (ETH, 2018).

3.3. Powertrain model in MatLab

The LHD powertrain setup described in chapter 2 is simulated in MatLab environment. An LHD powertrain is a complex piece of machinery so reasonable simplifications were made. The powertrain includes everything in between the battery and the wheels. Components such as transmission box and frequency converter are simulated with a constant efficiency factor. The simulation only includes the energy consumed by the traction motors. The steering circuit is omitted from the simulation because its power consumption is negligible comparing to the traction motors. The DDH circuit is also not simulated and modelled as a constant load. The work cycle is simulated as a linear motion in one-dimension. The load pick-up is instant and steering of the vehicle is incorporated into the linear movement.

A more detailed explanation of separate component modelling is presented in the following subchapters.

3.3.1. Duty work cycle

The standard duty cycles for most NRMM are undefined because of their vast variety and specific applications. Lehmuspelto (2010) defined a generic duty cycle for an LHD mining loader based on empirical data. The generic duty work cycle of an LHD mining loader is presented in figure 12. The LHD mining loader with an empty bucket drives 80m 4% uphill, 205m 12% uphill and then 55m on flat ground. The bucket is loaded with an extra 4000 kg at the loading place and the LHD vehicle drives back. The duty work cycle is realized as a

discrete point system that consists of a position change, a reference speed profile, upper and lower speed limits, the time elapsed and an inclination angle. This approach can be used for other similar applications as the parameters can be easily changed.

The actual duty cycle definition as a MatLab code is provided in appendix 4.1. The length of the total work cycle is 150 seconds with a time step of one second. The precision is high enough not to cause inaccuracies in the simulation while limiting the computation time. The experience shows that time increase depending on the simulation points is not exactly linear hence too small grids should be avoided. For a DP simulation, a reference or original profile is needed (providing an initial guess of the solution). The initial reference profile is defined as a combination of constant speed (5 m/s) and constant acceleration (1 m/s^2). To generate an optimal velocity profile a minimum and maximum limits are defined, which are 2.5 and 10 m/s respectively. By defining the limits for the velocity profile, a "wiggle room" is described, whose size also contributes to the total computation time. The total distance covered is calculated as an integral of speed function with respect to time. Position change at every second is required to run the DP function, which is defined in the duty cycle as well. The slope vector is split into two parts: before and after the loading of the machine. One fourth of the one-way distance the inclination is 0.04 rad, which corresponds to 4 % uphill. Half of the distance an inclination of -0.1194 rad (-12%) and the last quarter is movement on flat ground. The other half is symmetrical (flat – steep uphill – low downhill) as the LHD mining loader moves the same path backwards. Finally, the function is initialized and the motor efficiency values (appendix 3) are loaded. This model does not replicate the exact generic cycle in figure 13 but the precision is high enough to analyze DP performance. The duty cycle parameters are easily adjustable, making it suitable for different duty cycles.

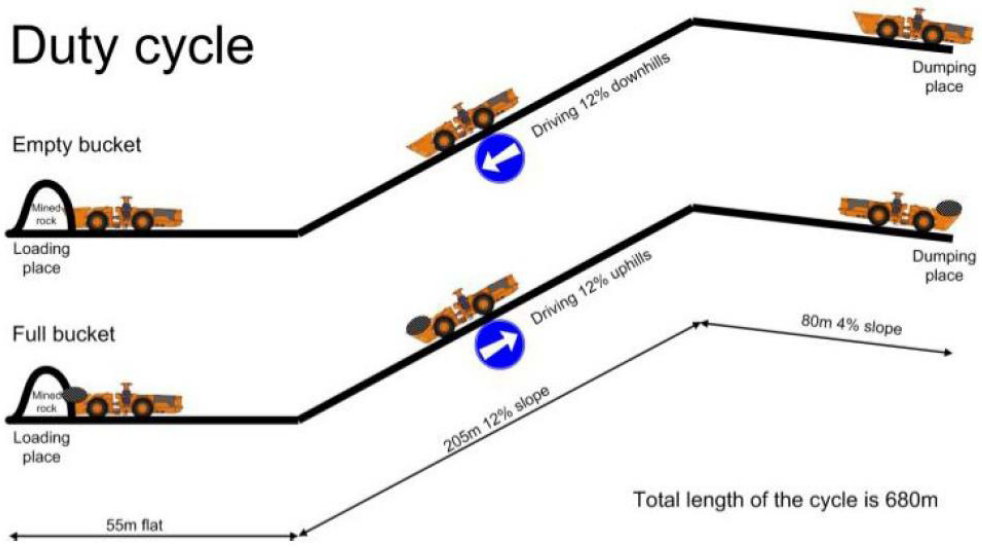

Figure 13: The duty cycle of the underground mining loader (Lehmuspelto et al., 2010)

3.3.2. Vehicle

The vehicle is modelled as seen in Figure 14. The drag force is ignored due to low speeds. The forces acting on the vehicle on a slope of α are shown according the 2nd Newton's law.

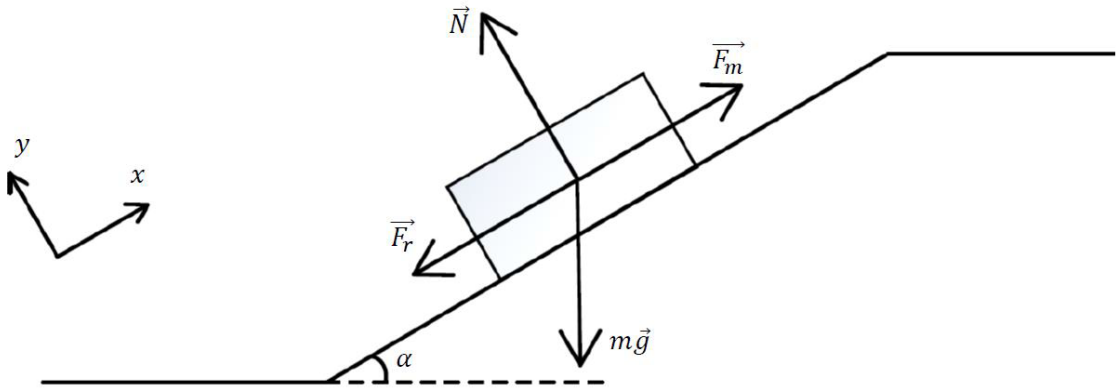

Figure 14: Vehicle model

$$\vec{N} + \overrightarrow{F_m} + \overrightarrow{F_r} + m\vec{g} = ma, \quad [14]$$

where $\vec{N}$ is the reaction force, $\overrightarrow{F_m}$ – the force exerted by the motor, $\overrightarrow{F_r}$ – the rolling resistance force, m – the mass of the vehicle, $\vec{g}$ – accelaration of gravity, a – acceleration of vehicle.

The forces are projected to x and y axes

$$x: \quad F_m - F_r - mg\sin\alpha = ma \quad [15]$$
$$y: \quad N - mg\cos\alpha = 0 \quad [16]$$

The wheel torque T_w is the product of the acting force and the wheel radius r_w. Wheel radius r_w is 0.62m (measured on the laboratory setup)

$$F_m = T_w / r_w \quad [17]$$

The rolling resistance force F_r is the product of the reaction force N and rolling resistance μ_r

$$F_r = \mu_r N \quad [18]$$

The rolling resistance μ_r is assumed 0.01 in this case.

From equation [16]

$$N = mg\cos\alpha \quad [19]$$

Equations [15] and [17] yield

$$T_w / r_w - \mu_r mg\cos\alpha - mg\cos\alpha = ma \quad [20]$$

Solving for T_w:

$$T_w = (mg\mu_r \cos\alpha + mg\sin\alpha + ma)r_w \quad [21]$$

where wheel speed in radians per second can be calculated as:

$$\omega_w = \frac{v}{r_w} \quad [22]$$

Wheel acceleration (rad/s^2)

$$a_w = \frac{a}{r_w} \quad [23]$$

Equations [20]-[23] are implemented in simulation that can be seen in appendix 4.4, "VEHICLE" section.

3.3.3. Motor

The performance of the electric traction motors is simulated as follows. Electric motor speed in radians per second is defined as:

$$\omega_m = k_g \cdot k_m \cdot \omega_w \quad [24]$$

here k_g is final drive gear ratio and k_m – motor belt drive gear ratio. ($k_g = 30.75$, $k_m = 2$)

Electric motor acceleration (rad/s^2)

$$a_m = k_g \cdot k_m \cdot a_w \quad [25]$$

Electric motor drag torque:

$$T_{m0} = I_{m0} \cdot a_m \quad [26]$$

where I_{m0} is motor inertia ($I_{m0} = 0.094$ as provided by the manufacturer)

Electric motor torque is calculated as:

$$T_m = \frac{T_w}{k_g \cdot k_m \cdot \eta_d} + T_{m0} \quad [27]$$

Here η_d is the total drivetrain efficiency. Electric motor efficiency η_m is interpolated from motor efficiency map provided by Siemens manufacturer. The full table of efficiency values can be seen in Appendix 3.

Electric power consumption/regeneration is calculated as:

$$P_m = \omega_m \cdot T_m \cdot \eta_m \quad when\ driving \quad [28]$$

$$P_m = \frac{\omega_m \cdot T_m}{\eta_m} \quad when\ breaking \quad [29]$$

The implementation of [24]-[29] can be seen in appendix 4.4 “MOTOR” section.

3.3.4. Battery

The battery is simulated as discussed in chapter 2.1.2, with a constant internal resistance of r. The power provided by the battery:

$$P_{be} = P_m + P_{aux} \quad [30]$$

where P_{aux} is constant power required for auxiliary systems (constant 10kW in this case).

Battery current is calculated:

$$P_{be} = UI - rI^2 \quad [31]$$

$$I_b = \eta_e \cdot \frac{U - \sqrt{U^2 - 4 \cdot r \cdot P_{be}}}{2 \cdot r} \quad [32]$$

where U is battery voltage and Coulombic efficiency when charging or discharging, $\eta_e = 0.98$ assumed in this case.

Battery power consumption P_b is used a cost function in DP algorithm.

$$P_b = I_b \cdot U \quad [33]$$

Equations [30]-[33] can be seen in appendix 4.4 “BATTERY” section.

3.4. Selecting variables and control signals for the optimization problem

The elapsed discrete time is selected as a state variable

$$x_{k+1} = f(x_k, u_k) + x_k, \quad k = 0,1, \dots, N-1 \quad [34]$$

With boundary conditions:

$$x_0 = 0, x_{max} = 167, \qquad x \in [x_0, x_{max}] \quad [35]$$

x_{max} is the length of the duty cycle following the reference speed profile in the final stage of the simulations.

u_k is the control variable which is used to determine the speed v_k.

$$u_k \in [0,1] \quad [36]$$

$$v_k = u_k(v_{max} - v_{min}) + v_{min} \quad [37]$$

$v_{max} = 10$ m/s and $v_{min} = 2.5$ m/s

The goal is to minimize power from battery:

$$\min_{u_k \in U_k} \sum_{k=0}^{N-1} P_b(u_k, k) \cdot T_d(u_k, k) \quad [38]$$

N is a variable step allowing better dynamic accuracy. In this case, $N = 167$ for a time step of 1 second.

To complete the modelling for debugging reasons, infeasibility matrix is defined and it consists of three conditions:

- Torque at the given speed is within limits defined by torque speed map:

$$T_{min} < T_m < T_{max} \quad [39]$$

- Battery current can only have real values (from equation [32]):

$$U^2 - 4 \cdot r \cdot P_{be} > 0 \quad [40]$$

- The acceleration of the vehicle is limited, which is defined by the maximum torque of the motor.

$$|a| < 3 \quad [41]$$

This chapter defined the method used for this case study – a DP optimization algorithm to minimize the energy consumption of the traction motors of an underground LHD mining loader powertrain. The method includes the description of DP in a general mathematic language, an application of a DPM tool developed for similar projects and a simplified model of a powertrain based on the Aalto laboratory setup. This thesis aim to prove that DP algorithm is a useful offline tool for NRMM energy consumption reduction. The results of the simulation are presented in the following chapter.

4. Results

This chapter will present several stages of LHD mining loader powertrain simulations results and discuss the issues relating to them. The simulations will be presented in a chronological order to show the process development. The simulations are rather time consuming and for the first dummy simulation stages, the generated grid was larger than initially planned and the duty cycle is slightly shorter than described in chapter 3.2.1. The first simulations were needed for code and model debugging reasons and checking if the algorithm compatibility. The final simulation is considered the actual results of this study.

The simulation consists of two optimization cycles. The first is the unloaded vehicle moving to the loading place. Most of the path is downhill, thus a negative power consumption can be expected for the first half-cycle. The second half is the loaded vehicle (4 tons added to the vehicle mass) moving the same path backwards. Going uphill with a heavier vehicle will result in a very high power consumption in the second half. The results are therefore split into two parts. The first is going to the loading place and the seconds is going back. In addition, the generated DP results are compared against a non-optimal speed profile composed of constant acceleration and constant speed. The results will show the power consumption per unit of distance (Wh/km) or energy efficiency and the total time elapsed which can be interpreted as work efficiency. Finally, the simulation limits and total simulation time are presented.

For each simulation, figures will present a velocity profile graph and motor efficiency map overlaid with electric motor duty cycle. The graph will also include the original (reference) velocity profile, the control variable u_k [36], which drives the speed function, and the battery system power, whose integral the DP function is trying to minimize. The efficiency map will show the general electric motor operation area.

4.1. Initial simulations

The very first simulations with the LHD mining loader powertrain model described in chapter 3.2 were unsuccessful. After a careful consideration, the main battery was concluded to be unsuitable for this operation. The Aalto battery could not provide enough power to drive 14-ton vehicle 12% uphill. Therefore, the model was changed to suit the simulation as several changes/simplifications were made. The battery capacity was increased four-fold to wield the traction motors enough power. In addition, the accurate simulations proved to be rather time consuming, thus the first experimental simulations are carried out with only approximate parameters for a shorter duty cycle.

The traction motors are assumed to be loaded evenly, whereas in real world applications, one of the motors is primary taking up the majority of the load while the second motor is auxiliary providing the torque in certain circumstances, for example, when the wheels slip or the axle is in mid-air. The load pick-up is instantaneous, while normally it can take several seconds. The hydraulic and steering circuit power consumption are not simulated and is included into constant auxiliary load.

The speed limit for most manned underground NRMM is 15 km/h = 4.167 m/s. For the sake of simplicity, the first simulations utilize 5 m/s speed limit and the duty cycle is shortened to 120 s and 31 points grid, to reduce the computation time. Final minimum and maximum half-cycle times are 50 and 72 seconds respectively (1.2 multiplier). The DP results are presented in the tables 4 and 5 below.

Table 4: 1st simulation – energy consumption

	Original results, Wh/km	DP results, Wh/km
1st half	-2467.5	-2475.0
2nd half	9733.2	9676.9
Total average	**3632.9**	**3601.0**

Table 5: 1st experimental simulation – time elapsed

	Original results, s	DP results, s	Simulation time, s
1st half	60	57.77	28.94
2nd half	60	61.17	58.19
Total	**120**	**118.94**	**87.13**

The first of the duty cycle is mostly driving downhill, thus the energy consumption is negative – the power is regenerated. For the second half, the loaded vehicle drives mostly uphill and the energy consumed is much higher. The total energy consumption was reduced from 3632.9 to 3601.0 Wh/km, only 0.89% decrease. The difference in the time elapsed, which can be interpreted as a work efficiency, is also insignificant. The DP optimal speed profile provide miniscule improvements for this scenario. The simulation time was tracked in order to evaluate the possibility of real-time applications. However, even for a shortened, less accurate duty cycle, the simulation time is too high. The DP algorithm is exceptionally an off-line tool.

Figure 15 shows the optimal velocity profile in blue, which is almost identical to the reference profile in black. The control function (black dots) ranges from 0 to 100, where 100 means the maximum change in the function and 50 – no change whatsoever. The dependence is not linear, though, i.e. 75 does not result in half the maximum acceleration. Energy storage

system (ESS) power is marked in red. ESS is the function that DP algorithm is trying to minimize, while keeping other parameters, such as speed and acceleration, within the limits.

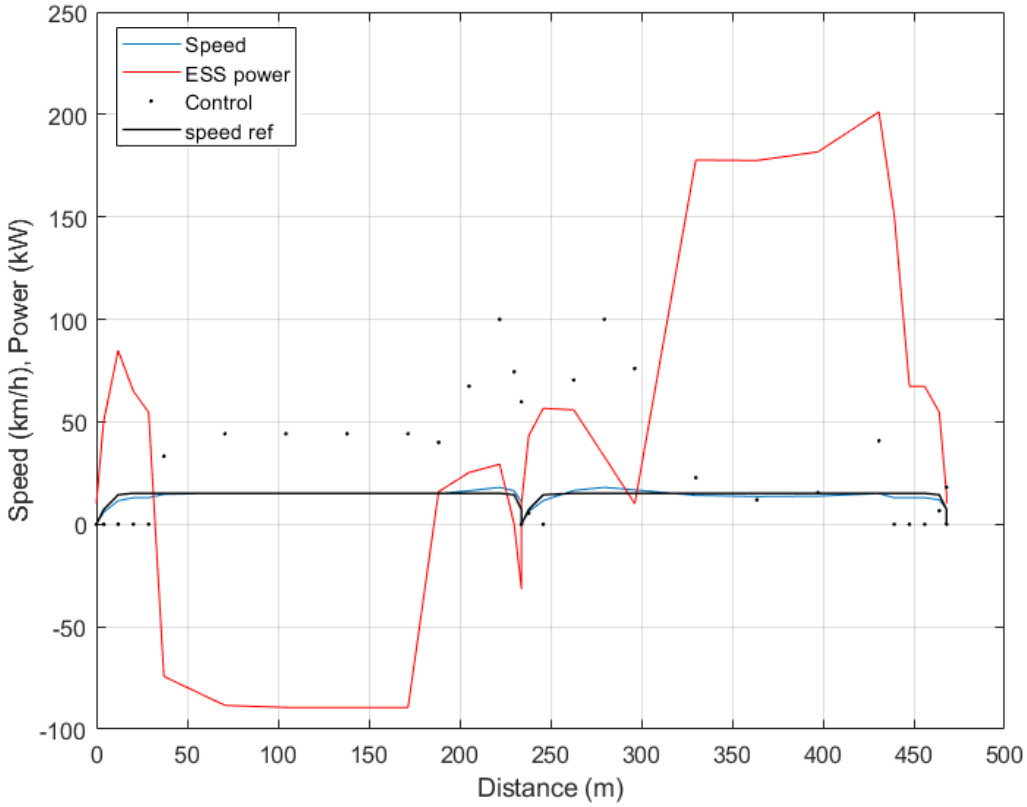

Figure 15: 1st generation speed profile

Two half cycles are clearly seen in the figure. The first half stats with a slow low inclination uphill movement followed by a lengthy downhill (power regeneration) movement and a slight acceleration before an abrupt stop. The loaded vehicle then drives all the way back consuming most power. The peak power demand is over 200kW, it is unsurprising that the present battery failed to provide enough power.

The figure 16 shows the electric motor efficiency map. It is a high-speed electric motor and has the best efficiency at the very high end of speed axis. However, due to low speed limits the motor is unable to reach high speeds. The vehicle speed of 5 m/s correspond to the motor speed of 4500 rpm with the current transmission configuration. The motor duty cycle (in black) shows that the motor is not operating at the highest efficiency area. The next generation simulations will attempt to provide better efficiency results by changing the limits of the model and allowing the motor to reach its highest efficiency area.

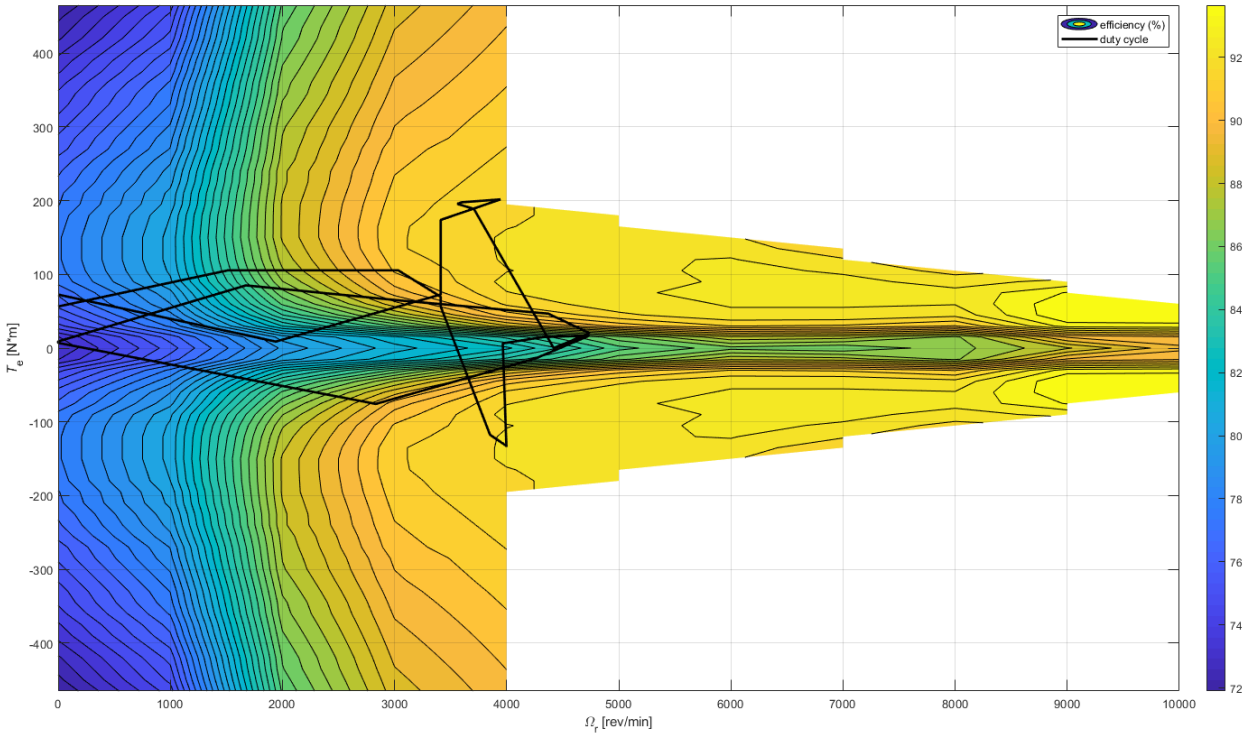

Figure 16: 1st generation motor duty cycle

4.2. Simulation with an increased speed limit

In order to achieve better results and to present the full capacity of DP function, the upper speed limit were increased up to 10 m/s and lower to 2.5 m/s. It allows more freedom for the function to search for the better results. The final half-time restrictions are also lowered to 30 s and 90 s (multiplier 2). The grid size remained the same – 31 points. The results of the second simulation are presented below.

Table 6: 2nd experimental simulation – energy consumption

	Original results, Wh/km	DP results, Wh/km
1st half	-2467.5	-2584.6
2nd half	9733.2	8391.5
Total average	**3632.9**	**2903.5**

Table 7: 2nd experimental simulation – time elapsed

	Original results, s	DP results, s	Simulation time, s
1st half	60	40.7	33.21
2nd half	60	57.9	66.99
Total	**120**	**97.6**	**100.20**

Increasing the speed limit for the simulation yielded significantly better results. However, figure 17 displays odd oscillations in ESS power and the validity of the choppy characteristics is questionable. The resolution is very low and the speed profile should be more precise in case of hidden oscillations.

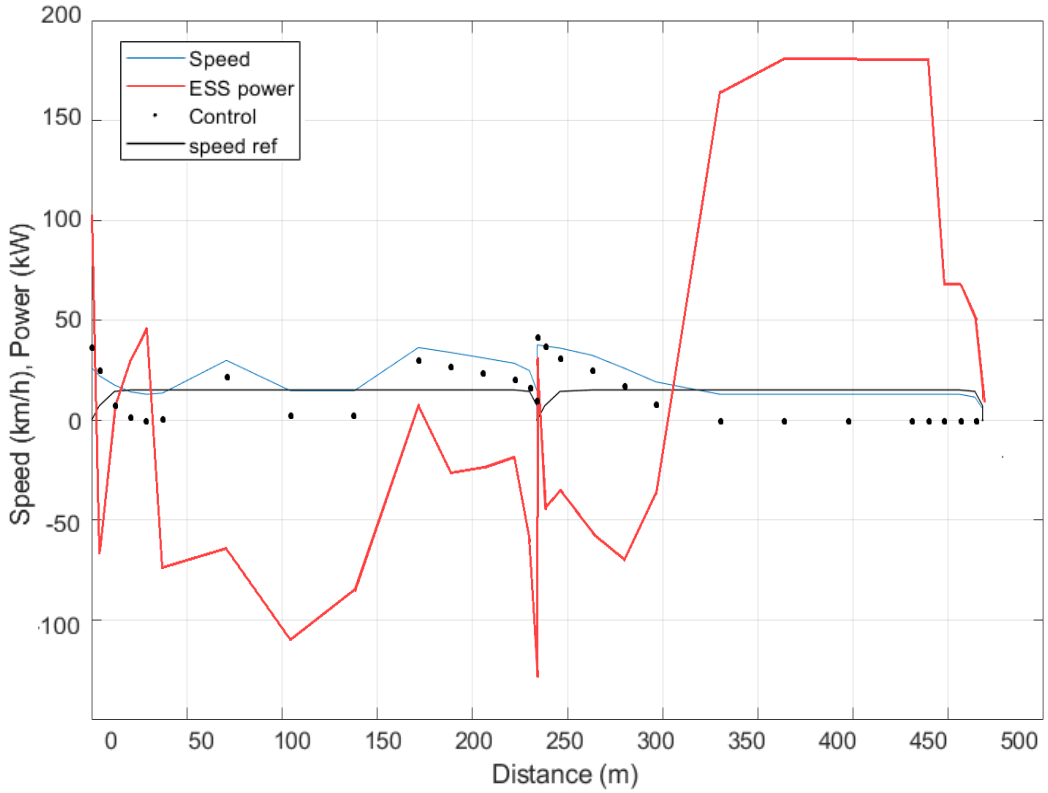

Figure 17: 2nd generation speed profile

Figure 18 proves that the motor operates over the entire T/w map and reaches the its highest efficiency areas. The DP program proved to be functional, thus the next simulation includes the full duty cycle with an improved accuracy – a smaller grid.

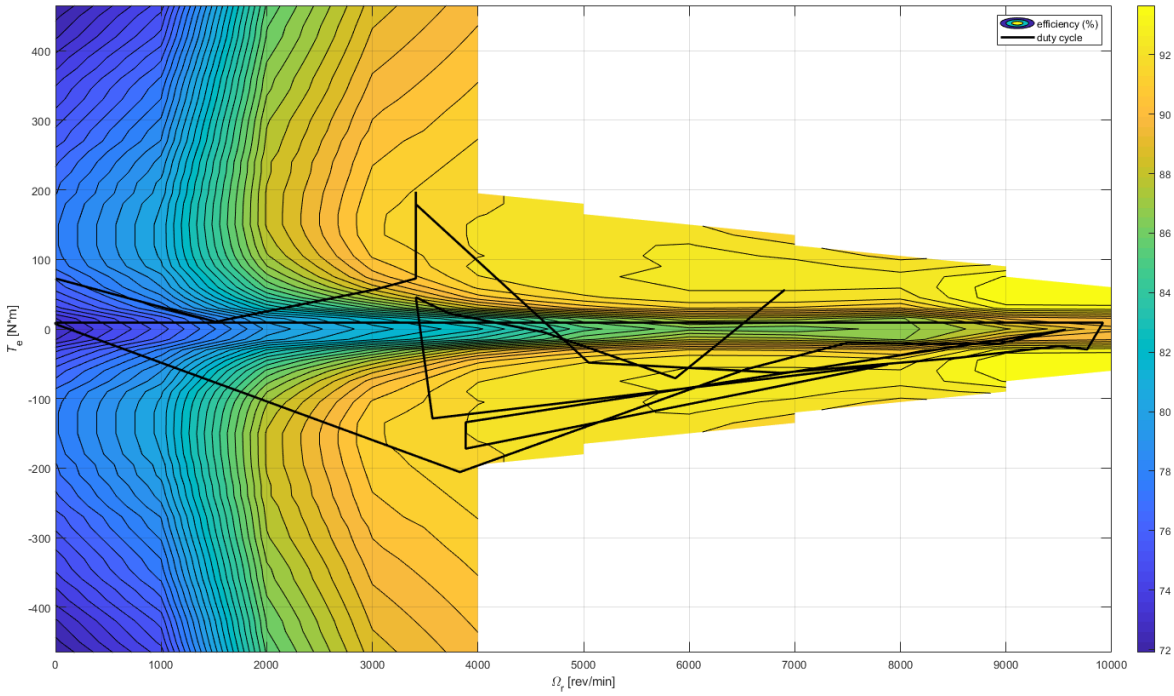

Figure 18: 2nd generation motor duty cycle

4.3. Simulation with an improved accuracy

The 3rd generation simulations features the same speed restrictions as in the previous simulations. The final half time restrictions 37.5 s and 150 s (multiplier 2). The grid size is increased to 75 points and model runs for the full duty cycle with a maximum reference speed of 5 m/s.

Table 8: 3rd experimental simulation – energy consumption

	Original results, Wh/km	DP results, Wh/km
1st half	-228.7	-1682.8
2nd half	13706.3	7421.9
Total average	**3632.9**	**2903.5**

Table 9: 3rd experimental simulation – time elapsed

	Original results, s	DP results, s	Simulation time, s
1st half	75	69.4	110.1
2nd half	75	75.9	229.2
Total	**150**	**145.3**	**339.3**

The results for the extended duty cycle are promising, the energy consumption decrease is rather significant and even the work efficiency increase is noticeable. However, a previously hidden oscillation appears during downhill part of the cycle, as seen in figure 18. The other parts of the parts profile are as expected. To deal with the oscillations, the next simulation penalizes the acceleration and increases the accuracy even further. The reason behind the oscillations is not perfectly clear. The DPM function does not have an elaborate error-handling feature. Therefore, it is highly probable that an unknown error causes the control function to reset to zero several times.

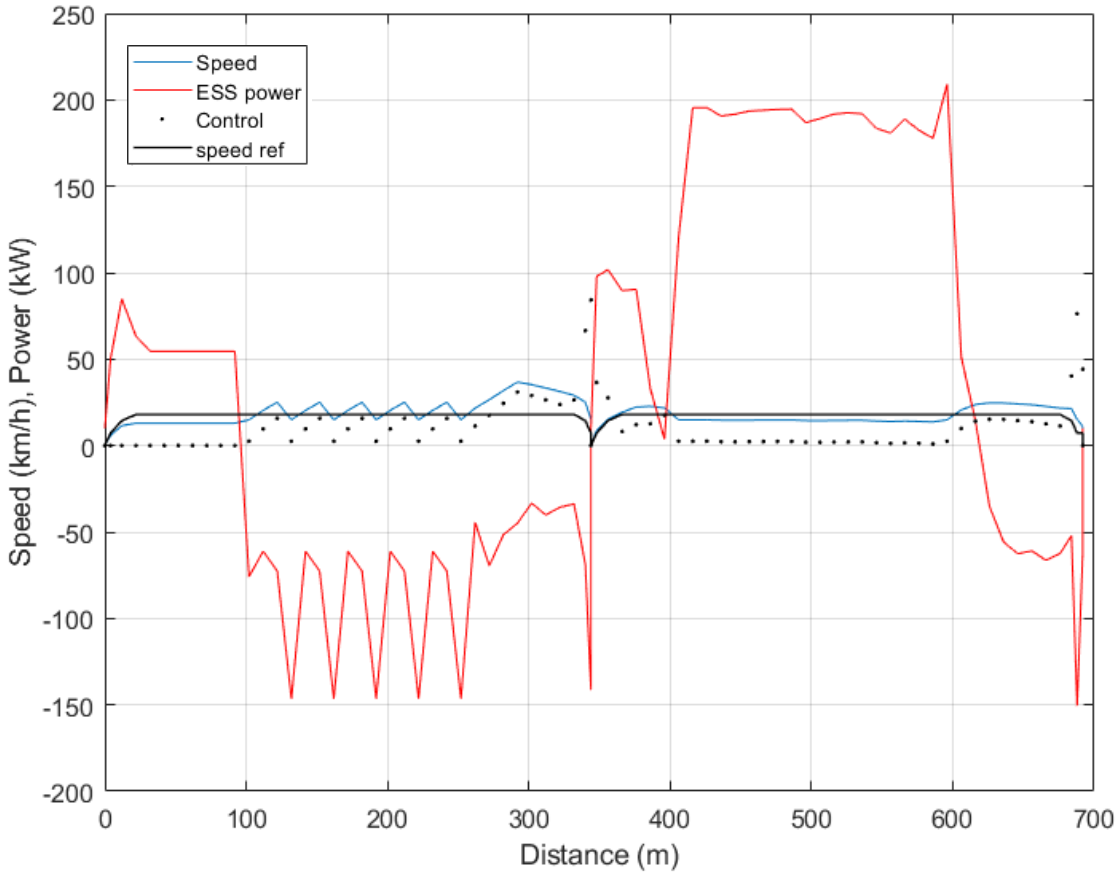

Figure 19: 3rd generation speed profile

4.4. Simulation with a penalized acceleration

The 4th generation simulations features the same parameter restrictions as in the previous simulations except the grid size was increased to 151 points (1 second time step) and a penalization of acceleration is introduced. It is supposed to deal with the oscillations during the power regeneration period. The acceleration is penalized in the cost function (see appendix 4.4).

$$C\{1\} = Pb/1e6 + acc. \qquad [42]$$

The equation means that 1 m/s in change of speed is as costly as 100 kW in power. Equation [42] does not have a physical meaning. It is a mathematical expression to minimize the total change in speed in the final solution. The acceleration penalty eliminated the oscillations as seen in figure 20. In addition, the accuracy of the simulation is enough to observe the trends in every section of the cycle.

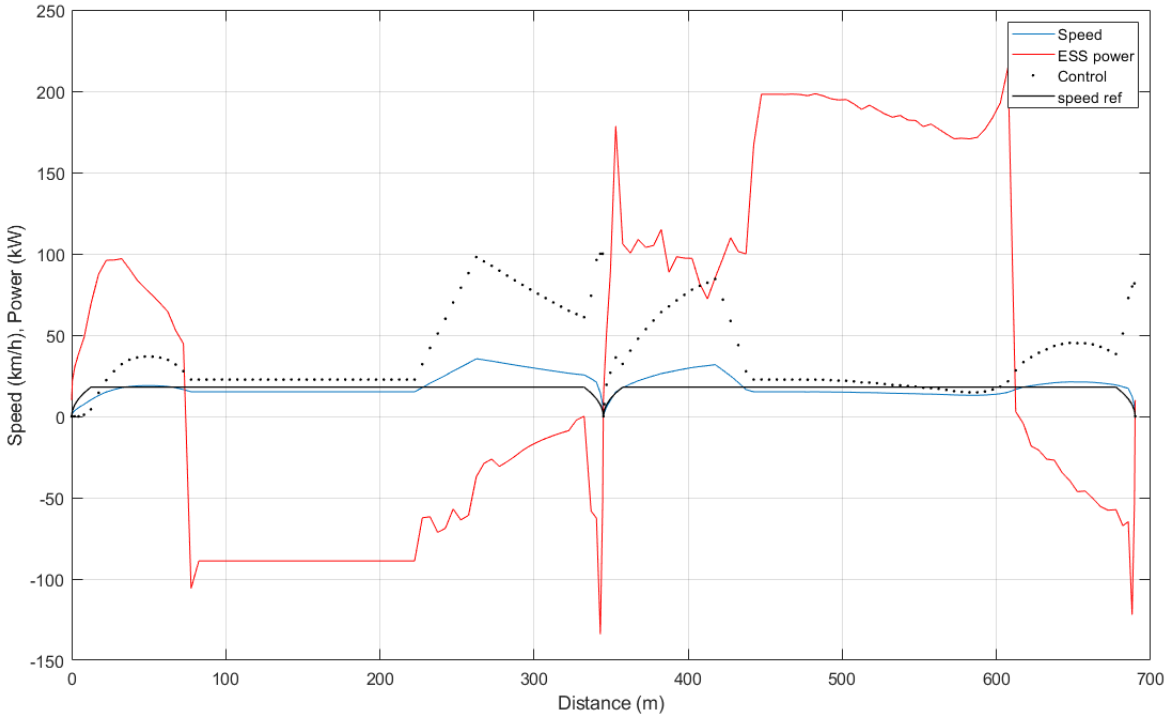

Figure 20: 4th generation speed profile

4.5. Final simulation

The previous simulations while not perfectly accurate, illustrated the method adaptability and its underlying issues. Nevertheless, it proved to be a viable off-line energy optimization tool. This subchapter will correct the minor modelling errors and present a comprehensive comparison to a redefined original speed profile.

The previously mentioned reference duty cycle consisted of a constant acceleration of 1 m/s^2 and a constant maximum speed of 5 m/s. However, is not entirely true for the case study

described in the chapter 2. The maximum available acceleration on flat ground is 3.08 m/s^2 and the maximum speed for underground load-haul-dump applications is 15 km/h or 4.166 m/s (Lehmuspelto, 2010).The definition of the duty cycle is clearer and can be seen in the appendix 4.1 whereas the previous simulations utilized custom imported Excel spreadsheets for every simulation.

Tables 10 and 11 present the simulation results. The simulated DP optimal speed profile is compared with a reference profile.

Table 10: Energy consumption

	Original results, Wh/km	DP results, Wh/km
1st half	-839.6	-1066.0
2nd half	5516.9	5316.2
Total average	**2338.7**	**2125.1**

Table 11: Time elapsed

	Original results, s	DP results, s	Simulation time, s
1st half	83.5	81.6	49.7
2nd half	83.5	84.2	97.8
Total	**167**	**165.8**	**147.5**

The total average energy consumption decreased by 9.1%, which is a noticeable improvement. The work efficiency increase, on the other hand, is miniscule but it is relevant for the sensitivity study in the following chapter. The total simulation time, again proved to be too long for any real-time applications.

Figure 21 visually represents the optimal DP speed profile and compares it with a reference duty cycle.

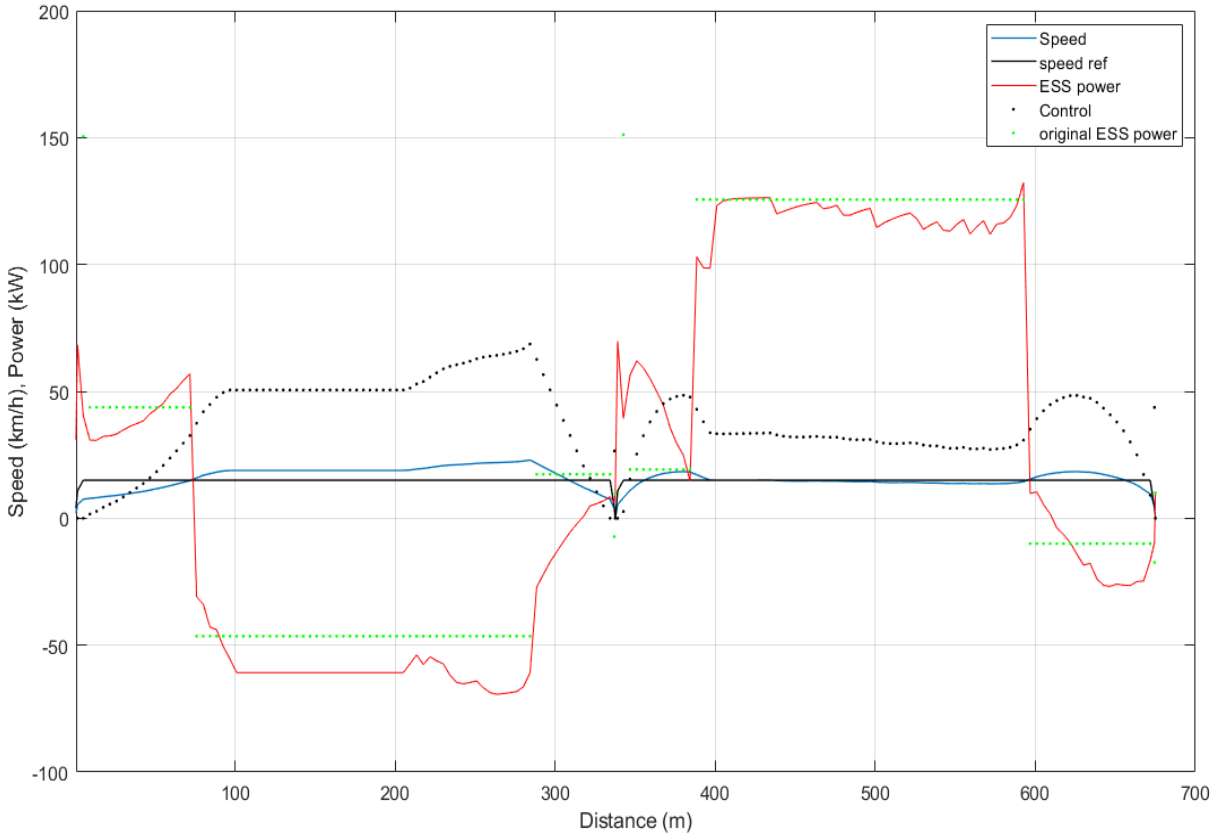

Figure 21: Optimal and reference speed profiles

The optimal speed profile in blue differs a lot from the reference profile in black. It starts with a slower acceleration almost reaching the lower speed limit. When the vehicle starts moving downhill, the algorithm suggests higher speed to increase energy recovery and a rather abrupt deceleration. This is defined by the actual coefficients of the acceleration penalization. The penalization coefficients are discussed in detail in the next subchapter. The second half cycle is less representative. The algorithm suggests slower acceleration and slightly higher speeds at low inclination intervals.

In contract to the previous simulations, the control signal avoids sudden changes in its value. The optimal speed profile is restricted by 36 km/h upper speed limit. However, the limit is never reached. This means that driving above 25 km/h is not efficient at any point of the duty cycle, thus increasing the limit would have no effect. The control signal never reaches the value of 100 – the change is never maximum, that makes it less harmful for the whole ESS. The figure illustrates the differences between the reference (red line) and DP optimal duty cycles (green dots). Visually the area under the curve is smaller for the DP speed profile for all sections except for part after the vehicle loading (340-385 on the distance axis) due to a sudden spike at the very beginning of the second half-cycle.

Figure 22 shows a different representation of the results. The duty cycle is shown on a speed-torque graph overlaid with the efficiency of the traction motors. The original duty cycle for comparison is noted with red dots. The motors operated according to a DP optimal cycle are operated at higher efficiency areas, decreasing the energy waste and theoretically reducing the motor overheating chance.

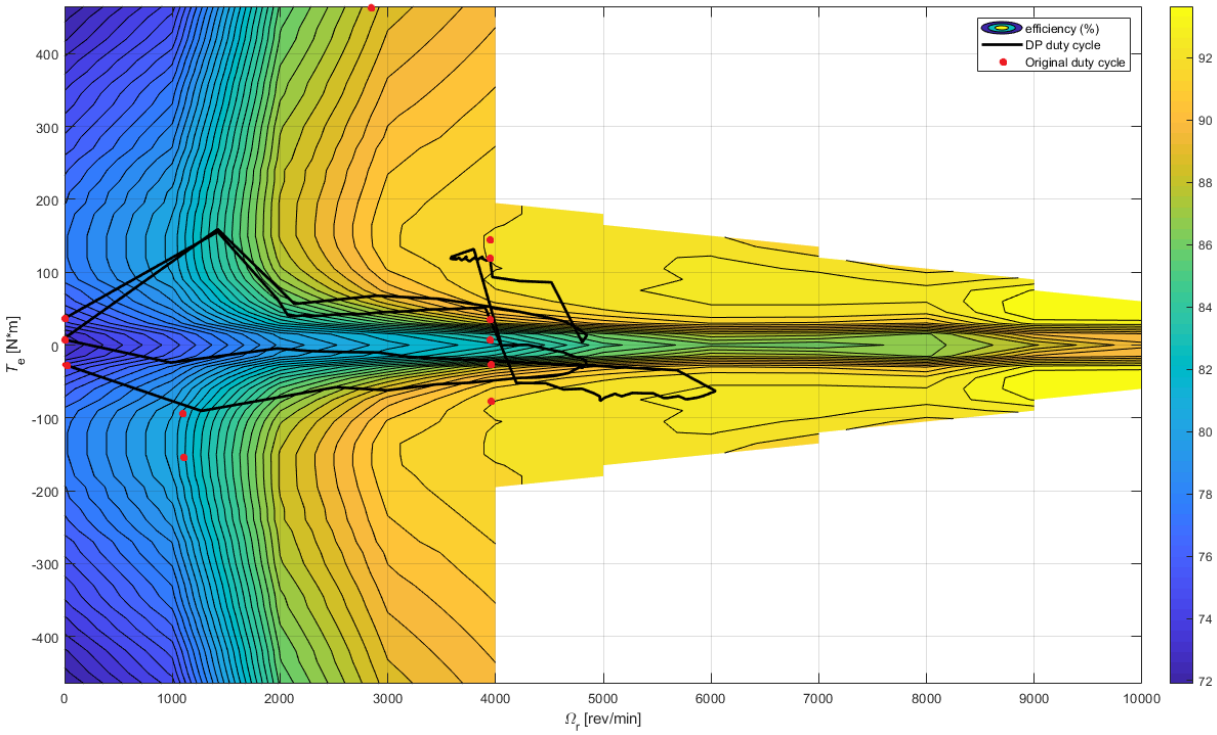

Figure 22: Speed-torque efficiency map with optimal and reference duty cycles

By applying DP algorithm, not only the energy efficiency significantly increased but also the electric traction motors are applied in their full capacity. The operating point for electric motors is moving all over the efficiency map, reaching the highest efficiency areas as seen in figure 20. Furthermore, the motors do not operate in over-torque regions (over 250Nm), which leaves a hefty safety margin for the calculation errors and an unexpected load increase in real world underground mine applications.

The use of DP algorithms is another advantage of utilizing electric powertrains for NRMM applications. Overall, with reasonable changes in limitations, DP can be a powerful tool to improve NRMM work and energy efficiency. As the parameters can be easily changed, the DP can be utilized for different duty cycles and even different types of powertrain, even a diesel powered. However, the results would not be as significant because only electric powertrains enable power regeneration, which is the key for improved energy efficiency.

4.6. Sensitivity analysis

The results of the simulations heavily depends on two variables that were inadvertently selected – the number of simulation nodes and the penalization coefficients. The more the simulation nodes, the more accurate the simulation is but it increases the simulation time. 167 simulation nodes were selected for the simulation, which corresponds to roughly 1 second time-step. The penalization was introduced to damp the sudden power spikes in the DP optimal speed profile. To introduce the penalization coefficients, the equation [42] is rewritten as:

$$C\{1\} = \alpha P_{batt}/10^6 + \beta a \quad [43]$$

4.6.1. Simulation nodes

The number of nodes in the DP problem increases the accuracy of the simulation. A more accurate power consumption simulation comes at a cost of a longer simulation time as seen in the figure 23. The total simulation time increases significantly with higher accuracy. After a certain point the trade-off becomes inadequate and the higher accuracy – unnecessary.

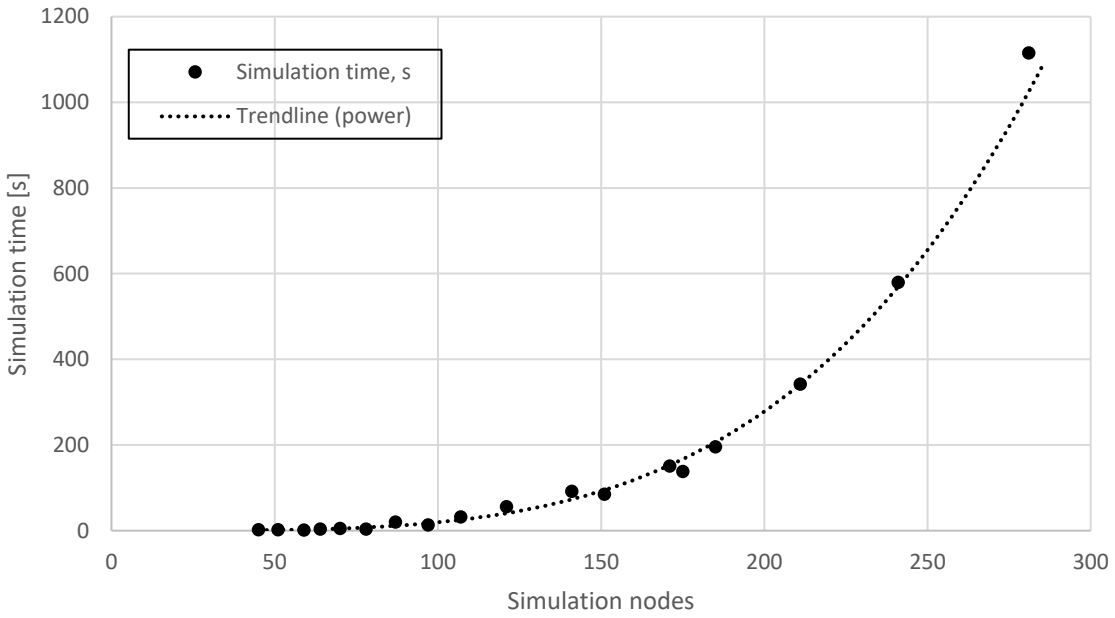

Figure 23: Simulation time dependency on the number of simulation nodes

Figure 24 presents the energy consumption dependency on the simulation nodes. The simulation results show rather large dispersion with a downwards trend. There is an oscillation in the simulation results. The red dot is excluded because it is counter-intuitive and it clearly does not follow the trend. Overall, increasing the number of simulation nodes does not provide significant improvement to the simulation.

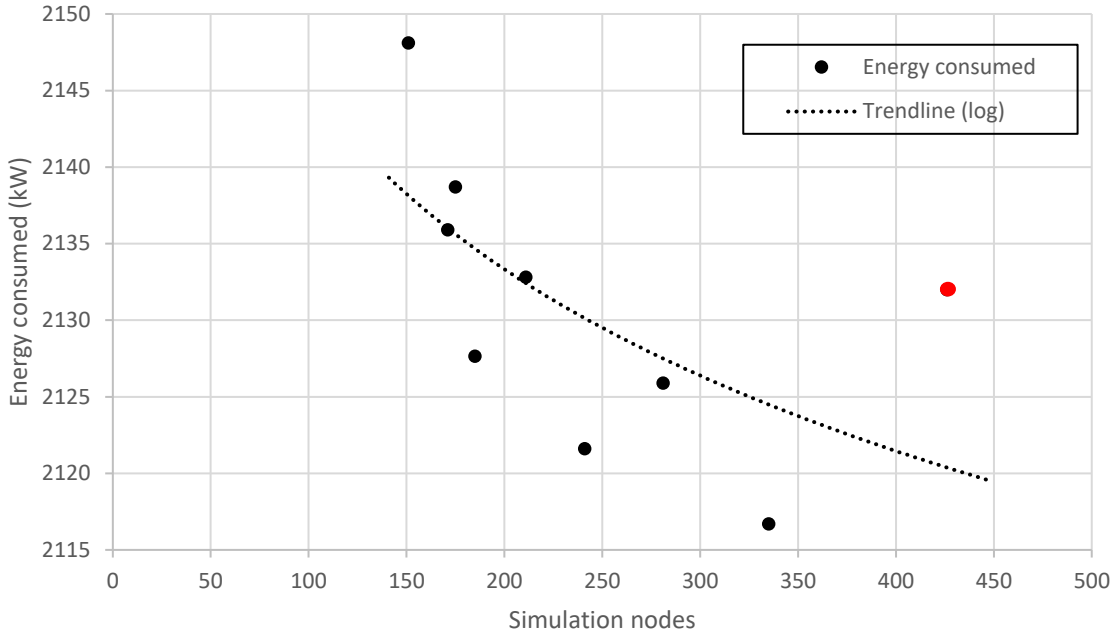

Figure 24: Energy consumption dependency on the simulation nodes

4.6.2. Acceleration penalization

The coefficients of equation [43] are normalized:

$$\alpha + \beta = 1 \qquad [44]$$

and presented in figure 25 as an argument of energy consumption and duty cycle duration. The increasing weight of α theoretically should increase the energy efficiency (black dots). However, the results are highly dispersed and only a slight downwards trend is observed. Therefore, the figure includes the duty cycle duration (brown dots) dependency on the coefficients. The duty cycle duration is reduces significantly with the increase of α. The value of β is harder to evaluate and it depends heavily on the exact situation but its involvement is necessary to avoid the oscillations displayed in the figure 19. Depending on the focus of the optimization – whether that would be energy or work efficiency, the coefficients can be selected accordingly. Introducing the penalization coefficients provides more flexibility for the optimization. Nevertheless, $\alpha = \beta$ is an adequate mid-point and represents this DP problem accurately.

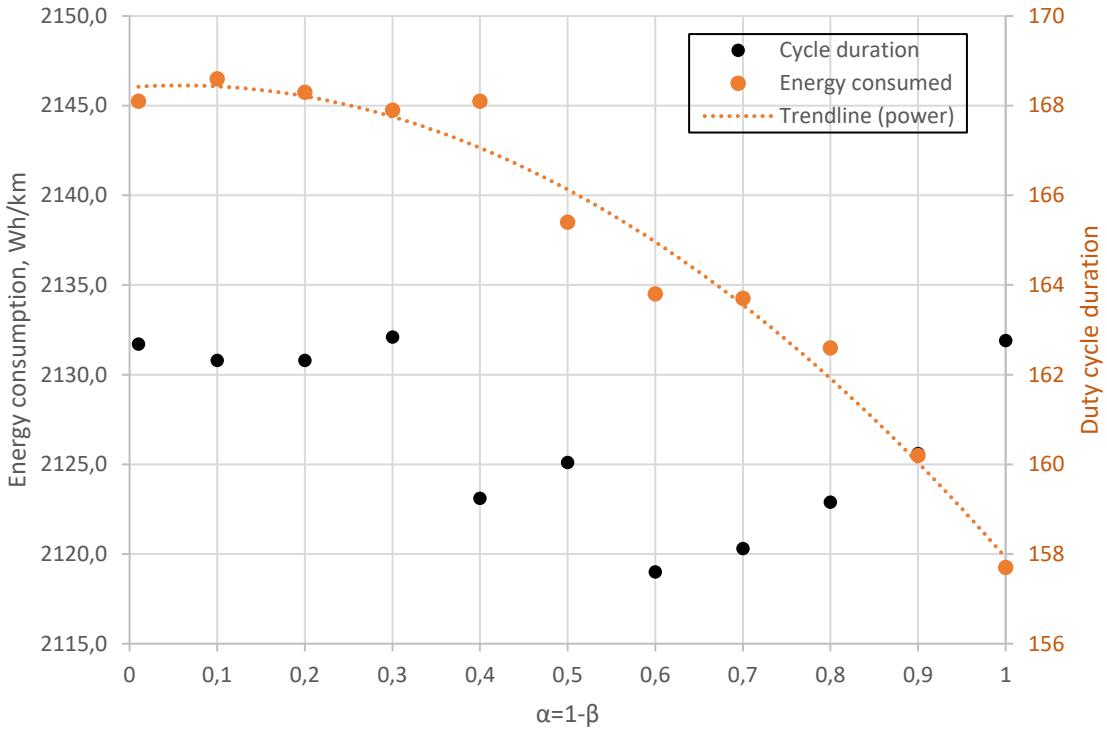

Figure 25: Consumption and cycle duration dependency on penalization coefficients

5. Discussion

5.1. Assumptions and conditions

NRMM electric powertrains are attractive due to the absence of local emissions, high power efficiency and compact size. The results of the chapter 4 presented another great advantage of electric NRMM powertrains - viability for optimization. The optimization algorithms can be applied for conventional powertrain models as well but it would be not nearly as effective. Lajunen (2013) showed efficiency increase for conventional buses while using DP function to optimize standard Braunschweig bus cycle. However, NRMM does not have standard duty cycles and the ones that are defined are not nearly as complex as Braunschweig cycle for city busses. Complex duty cycles with many acceleration-deceleration sub-cycles present more room for improvement and the generic LHD duty cycle lacks the complexity thereof. To deal with the simplicity of the cycle and to produce satisfactory results, the speed limit was increased for LHD mining loader model. A speed limit increase up to 10 m/s is a huge factor for work efficiency of material transportation. The results showed increased proposed speed but it does not increase infinitely and settles at around 25 km/h in the final simulation. Overall, the implementation of optimal DP velocity profiles require some level of mine automatization because a human vehicle operator is unable to follow the velocity profile closely. The speed limit is specified for the human workers safety, in other words – to minimize the chance of human error. Hence, semi-automatized approach is necessary for this study, which allows the changes in speed limit and therefore a successful implementation of DP velocity profiles.

Although the DP algorithm focuses on energy efficiency optimization, the results of the 3rd generation simulation presented a possibility for an increased work efficiency as well. By changing the cost function accordingly, prioritizing the cycle time, the work efficiency or time elapsed for duty cycle can be optimized. Usually, work efficiency and energy efficiency are inversely proportional – if the work efficiency increases, the energy efficiency decreases and vice versa. Decision whether work or energy efficiency is the focus must be made according to specific economic based studies. In any case, DP provides a choice for optimization focus.

5.2. Model inaccuracies

A deterministic model of LHD mining loader was simulated to test the performance of DP algorithm. However, as any other model, it involves certain simplifications and assumptions. The speed drag is ignored in the simulation due to speeds under 10 m/s, thus it does not create large inaccuracies (Beckman, 1991). However, other variables, not constant in the real world, might have an effect on overall results. For example, the wheel-rolling coefficient (0.01 in this case) is assumed constant throughout the work cycle. The roughness of the road and rubble affect the grip of the tires. Thus, it is impossible to simulate the motion with a perfect accuracy. The grip of the tires is a major factor on power consumption. Nevertheless, both optimal and non-optimal profiles operate in the same circumstances, so the comparison between the two is fair.

The over torque area is also needed for taking into account the load pick-up period. The machine operators usually ram into the rubble to slide the bucket under the rocks to pick up

the load. While it not very time-consuming, the traction motors are strained heavily. In addition, the pick-up is not always exactly 4 tons, which would result in more obscurity in the work efficiency estimations. In addition, the powertrain energy consumption heavily depends on the load size because of the movement uphill, which is the most consumption-heavy periods of the duty cycle.

Other simplifications, already mentioned in previous chapters, includes the traction motor loading and the battery capacity. Both traction motors are considered evenly loaded, even though in the real world applications, the primary motor is usually loaded more than the secondary. Thus, the actual duty cycle of the primary motor would be slightly higher than the simulated. The simulation leaves a large margin for the operational torque region and as an electric motor can be overloaded for short amount time, proving the simplifications to be well reasoned. The extra battery packs were not accounted for in the simulation. Extra five battery packs could weigh as much as 500kg.

The gearbox was not simulated as it is normally operated by the vehicle driver and the DP algorithm is unable to simulate the gear switches. VFD were simulated with a constant coefficient of 98%, although it can drop as low as 91% for the lowest motor speed (Appendix 3). Nonetheless, the motor is operated at higher speeds, where the VFD efficiency is not a deciding factor. Overall, the results are satisfactory and it makes a strong argument in favor of electric powertrains.

The importance of energy efficiency for electric motors does not only lay in electricity consumed (kWh). The cost of electrical power is much lower than the price of fossil fuels and while extra savings are desirable, an electric powertrain will have cheaper power consumption than conventional powertrains even without an optimal velocity profile. An increased overall motor efficiency provides indirect maintenance savings. It prolongs the battery lifetime and minimizes the charging cycles per work completed (material moved). In addition, if the electric motor is less efficient, due to the laws of thermodynamics, the more unused energy is converted into heat. High temperatures increase the risk of failures and might require advanced cooling systems, which, in turn, would increase the initial investment costs.

Despite the model inaccuracies and the necessary assumptions, the simulation provides sufficient results to analyze the performance of an electric powertrain of an LHD mining loader. Electric powertrains allow duty cycle automation, which enables the use of DP algorithms as DP proved to be a useful tool to increase the energy efficiency over a specified duty cycle.

5.3. Technical difficulties

The unearthed HV electric systems are potentially dangerous. Since there is no actual connection to the ground (earthing), the negative potential is floating with respect to the actual ground. Thus, a potential difference might exist between the chassis of the vehicle and the earth. For this reason, a Bender isometer is used for EL-Zon project case study. An isometer is a device that measures the resistance between the life parts of the setup (busbars) and the chassis. It measures the leakage currents every time the VFD is enabled and it is a part of the protection system.

Another part of the protection system is the safe-torque-off (STO) circuit. STO disables the VFD if the electric motor (or other spinning parts) are uncovered. The parts that should be included in the protection circuit include the traction motors, the belt drive and the main power shaft. Although all the spinning parts are covered or not moving when the vehicle is stationary, STO implementation is highly recommended (ABB communication, 2018).

The battery mains are protected by DC fuses and a set of contactors. However, if the battery is partially discharged, in case of a failure, short circuit current might fail to blow the DC fuse. In addition, li-ion batteries are susceptible to sudden voltage changes especially during charging. Large inertia of LHD loader creates sudden voltage surges that might damage the battery. Therefore, brake chopper and brake resistor is needed. Normally the battery packs require a uniform charging voltage, the energy regeneration might prove to be difficult and serious power electronics are needed for this case.

The battery is the most vulnerable part of the powertrain. Moreover, electric powertrain development is heavily dependent on the battery research. Recently developed fast and ultra-fast charging systems are necessary for electric LHD powertrains. Otherwise, a spare battery set is needed to run the machine continuously. Nevertheless, that is not the case for all NRMM because they are constructed very differently and have varying duty cycles. For example, an underground concrete spraying machine has a very different duty cycle from LHD loaders. They tend to be stationary for long times (around 30 minutes), which can be used for battery charging while the machine sprays the concrete.

5.4. Specialized LHD powertrain motors

Currently there is no specialized motor for the LHD traction applications. Manufacturers choose the traction motors from the ones available in the market but there is no optimal choice. “GHH Fahrzeuge” (2018) employs a three-phase asynchronous motor with a rated

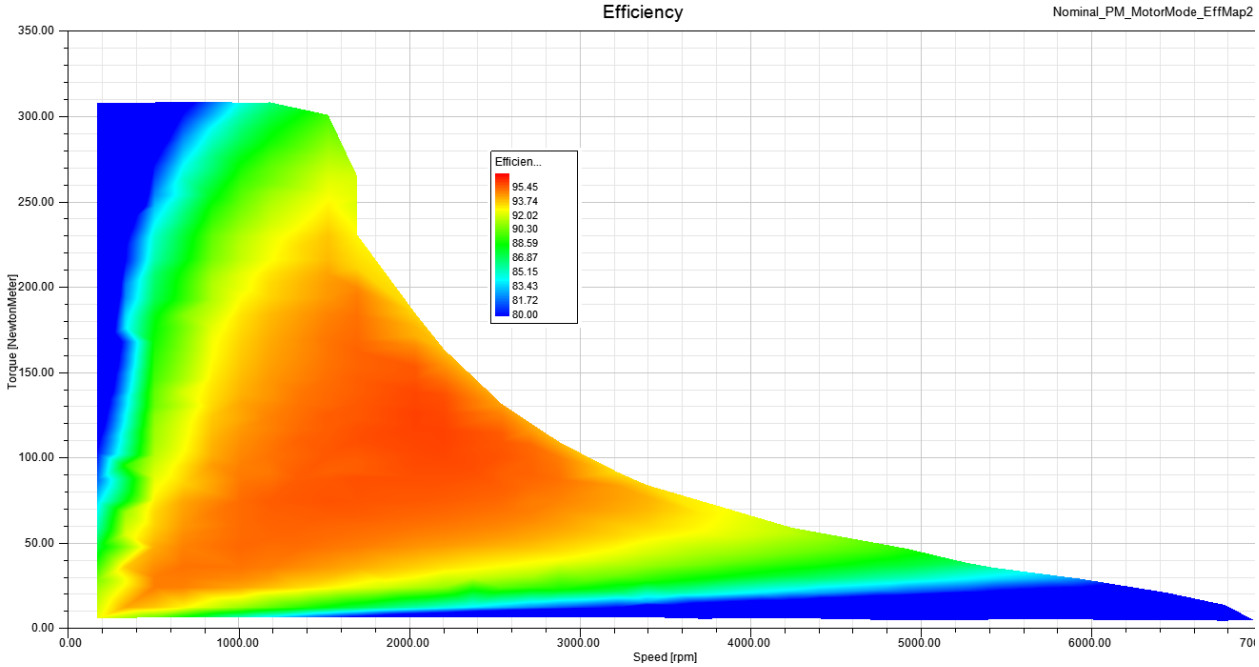

Figure 26: Efficiency map of a three-phase internal permanent magnet motor (Ansys blog, 2018)

speed of 1480 rpm. It is the same type of electric motor that is used in this case study. However, the nominal speed is lower, thus the gear ratio has to be increase to provide the same amount of torque. "Artisan vehicles" (2018) applies a synchronous permanent magnet three-phase electric motor with 4000 rpm rated speed. In comparison to the Aalto case study, motors have similar rated speeds but the types are fundamentally different. While synchronous machines are considered more efficient overall, they are more expensive and require an additional DC power source for energizing the rotor winding. A typical efficiency map of permanent magnets are significantly different from asynchronous motors, as seen in figure 21.

The permanent magnet motor is the most efficient at lower speeds, while induction motor, used in a case study, is the most efficient at high speeds. The permanent magnet motor has a rather large uniform maximum efficiency area but outside it, the efficiency drops significantly. Thus, the motor use in high speed and high speed is limited. The DP simulation with permanent magnet traction motors would yield entirely different results. The algorithm would try to remain at lower speeds as the efficiency is greater there. In addition, synchronous electric machines perform better as generators. During the power regeneration period, the voltage surges would be smoother and the inrush current would be lower.

6. Conclusions and future work

6.1. Conclusions

This thesis discovered an application of the DP algorithm – the energy consumption reduction of an LHD mining loader powertrain. An energy-optimal speed profile demonstrated a 9.1% decrease in energy consumption for a generic duty work cycle.

This thesis addressed the issue of harsh working conditions in the underground mines. Globally, the air quality improvement is enforced by tightening emission standards for NRMM. This paves the way for an influx of electric powertrains in underground mines for their numerous advantages including no local emissions and low noise levels. The viability of electric powertrains is based on health, environmental as well as economic factors. While alternatives such as hybrid powertrains are available, the economic incentive is greater for the fully electric LHD vehicles. The efficiency of the LHD electric powertrains was further improved by utilizing the DP algorithm. It was realized by creating a model of a real-size LHD vehicle prototype in MatLab and defining its empirical duty cycle. As the major part of the energy is consumed by the traction motors, the optimization algorithm causes them to be operated at a higher efficiency area, reducing the overall energy consumption.

DP algorithm is a powerful and universal offline tool for energy optimization. By presenting successful results, this thesis prompts many potential research topics relating to DP applications and further development of the LHD mining loader case study.

6.2. Future work

The MatLab simulation discussed in chapters 3 and 4 concentrates on minimizing the average power consumption for the duty work cycle. Occasionally, the energy consumption is not as relevant as work efficiency, especially considering low electric power prices. The work efficiency optimization can be achieved by changing the cost function and prioritizing the time elapsed over the energy consumption. To further improve the optimization process, certain coefficients could be introduced to calculate energy efficiency and work efficiency tradeoff, i.e. what is more important and by how much. These calculations would be based on the economic aspect and the unique application of NRMM in question. However, the duty cycle and the model of NRMM must be improved and adjusted accordingly.

In addition, the modelling process can be improved, which could include air drag simulation for an increased accuracy, steering and work hydraulics simulation, traction motors load simulation and a gradual change in inclination change in duty cycle description. The gearbox mechanics were not simulated as well, as it is normally operated by the vehicle driver. The current DP algorithm is unable to simulate gear switches. Conditional “if’s” would be possible to simulate the gear switch when the required load reaches a certain torque value, the operation area is too inefficient, or the motor is overloaded for too long. However, it would not contribute significantly to already existing results. Nevertheless, it could be a great platform for an implementation of artificial intelligence based on neural networks. The gear switching could be based on driver’s preferences as well as maximum efficiency.

This thesis is based on the case study where all the equipment is preselected. A future study could select a different mining loader setup with different type of traction motors and gears. Since permanent magnet electric machines are more suited to operate as generators, the energy regeneration could be improved. In addition, the DP optimization can be used for conventional NRMM solutions. A recent study by Heikkilä (2018) applies exactly the same DP optimization method described in this thesis for NRMM hydraulics i.e. booms and buckets. That approach can be applied for the direct driven hydraulics of the LHD mining loader.

7. References

ABB, 2015, *Product manual, HES880-104 converter modules*

ABB customer support, 2018. *E-mail communication*. 2018.07.02
FI-HES880.support@abb.com

Ansys blog, 2018. *Efficiency Maps for Electric Motors Made Easy.*
Retrieved: 2018.11.28
https://www.ansys.com/blog/efficiency-maps-for-electric-motors-made-easy

Artisan Vehicles, 2018. *Artisan's Battery-electric 4 tonne LHD.*
Retrieved: 2018.11.28
https://www.artisanvehicles.com/a4/

Back, M. 2004, *Predictive powertrain control for hybrid electrical vehicles,* IFAC Proceedings Volumes, Volume 37, Issue 22, April 2004, pp. 439-444.

Beckman, B. *Part 6: Speed and horsepower.* The physics of Racing
Retrieved: 2018.11.26.
http://phors.locost7.info/phors06.htm

Bellman, R. (1958). *On a routing problem*. Quarterly of Applied Mathematics. Pp. 87-90.

Bertsekas, D. 2005 *Dynamic Programming and Optimal Control Vol. 1. Third edition*

Brake, R. 2006, *The Importance of Underground Mine Ventilation.* Bulletin. Feature-Mine Ventilation. March/April 2006.

Buchmann, I. "Battery University", 2010, *Understanding Lithium-ion.* Retrieved: 2018.10.24.
https://batteryuniversity.com/learn/archive/understanding_lithium_ion

CSS electronics, 2018, online video. *CAN BUS EXPLAINED - A SIMPLE INTRO (2018).* Retrieved: 2018.10.25
https://www.csselectronics.com/screen/page/simple-intro-to-can-bus/language/en

Demain, E, 2011, online course. *MIT 6.006 Introduction to Algorithms, Fall 2011.*
Retrieved: 2018.10.29
https://www.youtube.com/playlist?list=PLfMspJ0TLR5HRFu2kLh3U4mvStMO8QURm

Dieselnet, 2013, *Braunschweig city driving cycle.* Emission Test Cycles.
Retrieved: 2018.11.15.
https://www.dieselnet.com/standards/cycles/braunschweig.php

Dieselnet, 2016.11, *EU: Non-road Engines.* Emission Standards.
Retrieved: 2018.10.24
https://www.dieselnet.com/standards/eu/nonroad.php

IARC, 2012 *Diesel Engine Exhaust Carcinogenic*. World Health Organization. International Agency for Research on Cancer.
Retrieved: 2018.10.24.
https://www.iarc.fr/en/media-centre/pr/2012/pdfs/pr213_E.pdf

Electrek, 2018. *Ultra-fast charging battery' tech secures $20 million investment from British oil giant BP.* 22nd of May 2018
Retrieved: 2018.10.24.
https://electrek.co/2018/05/22/ultra-fast-charging-battery-tech-storedot-investment-oil-giant-bp/

ETH, 2018*, Institute for Dynamic Systems and Control – Downloads*.
Retrieved: 2018.10.26.
http://www.idsc.ethz.ch/research-guzzella-onder/downloads.html

Innovative Vehicle Institute, 2019. *Updated configuration of a hybrid mining loader.* Flotte Rechargeable.
Retrieved: 2019.01.31
http://www.ivisolutions.ca/en/portfolio-items/updated-configuration-hybrid-mining-loader/

Jacobs, W. 2013, *Electric LHDs in Underground Hard Rock Mining: A Cost/Benefit Analysis*. Final Year Project Thesis, School of Mechanical an Chemical engineering, University of Western Australia.

GHH Fahrzeuge, 2018. *LHD LF-10HE.* Technical specifications
Retrieved: 2018.11.28.
http://www.ghh-fahrzeuge.de/en/products/lhd/electric-lhds/lf-10he/

Grimaldi, R. 2000, *Nonhomogeneous Recurrence Relations.* Section 3.3.3 of Handbook of Discrete and Combinatorial Mathematics. CRC Press

Hayes, 1996. "9.4: *Recursive Least Squares. Statistical Digital Signal Processing and Modeling*. Georgia institute of Technology. John Wiley & Sons.

Havells, 2016, *IE2 & IE3 Energy Efficient 3 Phase LV Induction Motors.*
Retrieved: 2018.10.24.
https://www.havells.com/content/dam/havells/brouchers/motors/Prima%20Series%20Motors/Prima%20series%20motor%20Catalouge.pdf

Heikkilä M. et al. 2018. *Fuel efficiency optimization of a baseline wheel loader and its hydraulic hybrid variants using dynamic programming*. BATH/ASME 2018 Symposium on Fluid Power and Motion Control. Bath, UK, September 12–14, 2018

Heninger, A. 2013. *Unicode Line Breaking Algorithm Technical Reports*. Technical Reports. Annex #14.
Retrieved: 2018.11.15
https://www.unicode.org/L2/L2013/13022-uax14-31.pdf

Jarkko, N. 2015, *Energy Efficiency Analyses of Hybrid Non-Road Mobile Machinery by Real-Time Virtual Prototyping* - Doctoral Thesis, Lappeenranta University of Technology.

Komatsu, 2018, *Hybrid loaders Joy 22HD.* Retrieved: 2018.10.24.
https://mining.komatsu/product-details/joy-22hd

Lajunen, A. et al., 2016. *Electric and hybrid electric non-road mobile machinery - present situation and future trends.* World Electric Vehicle Journal. 8. p. 172-183.

Lajunen, A. 2013, *Energy-optimal velocity profiles for electric city buses,* The 25th World Battery, Hybrid and Fuel Cell Electric Vehicle Symposium & Exhibition

Lajunen, A. *2010, Energy consumption simulations of a conventional and hybrid mining loader.* IEEE International Conference on Automation Science and Engineering, pp. 886-891.

Lehmuspelto, T., et al. 2010, *Modular driveline concept for underground mining loader.* World Electric Vehicle Journal, pp. 165-170.

Lehmuspelto, T. et al. 2015, *Full-scale Series Hybrid Mining Loader with Zonal Hydraulics.* Nordic Electric Bus Initiatives 2 & Electric Commercial Vehicles final seminar. Helsinki, Finland.

Liljestrom, J. 2014*, Electromehanical transmission challenges in non-road mobile machinery drivetrains*- Master's Thesis. Aalto University.

Manzi, P, 2018, *Market Beat, January 2018.* Nada.
Retrieved: 2018.10.24.
https://www.nada.org/nadamarketbeat/

Mensing, F. et al. 2013 *Vehicle trajectory optimization for application in eco-driving.* IEEE Vehicle Power and Propulsion Conference, 6-9 Sept. 2011, Chicago, IL, USA

Minav, T. et al. 2016 *Series Hybrid mining loader with zonal hydraulics,* Nordic Electric Bus Initiatives 2 & Electric Commercial Vehicles final seminar. Helsinki, Finland, 2016.

Official Journal of the European Union, 2003. *DIRECTIVE 2003/10/EC OF THE EUROPEAN PARLIAMENT AND OF THE COUNCIL of 6 February 2003 on the minimum health and safety requirements regarding the exposure of workers to the risks arising from physical agents (noise).*
Retrieved: 2018.10.24

https://eur-lex.europa.eu/LexUriServ/LexUriServ.do?uri=OJ:L:2003:042:0038:0044:EN:PDF

Paraszczak, J. 2014. *Electrification of Loaders and Trucks – A Step towards More Sustainable Underground Mining*. International Conference on Renewable Energies and Power Quality (ICREPQ'14) Cordoba (Spain), pp. 81-86.

Sundstrom, O. and Guzzella, L., *A Generic Dynamic Programming MatLab Function*, In Proceedings of the 18th IEEE International Conference on Control Applications, Saint Petersburg, Russia, 2009, pp. 1625-1630,

Tatiya, R.R. 2013, *Surface and underground excavations – methods, techniques and equipment.* CRC Press, Taylor and Francis Group. Bota Raton, Florida.

Tuck, M. 2011, *SME Mining Engineering Handbook*, *Third edition*. Society for Mining, Metallurgy and Exploration, Inc. Printed in United States of America.

Turunen, A et al, 2018, *Experimental Investigation of Direct Drive Hydraulic Units Implemented in a Mining Loader.* IEEE Global Fluid Power Society GFPS2018. Samara, Russia, July 18-20, 2018

Appendix 1: Models of DDH bucket and boom units.

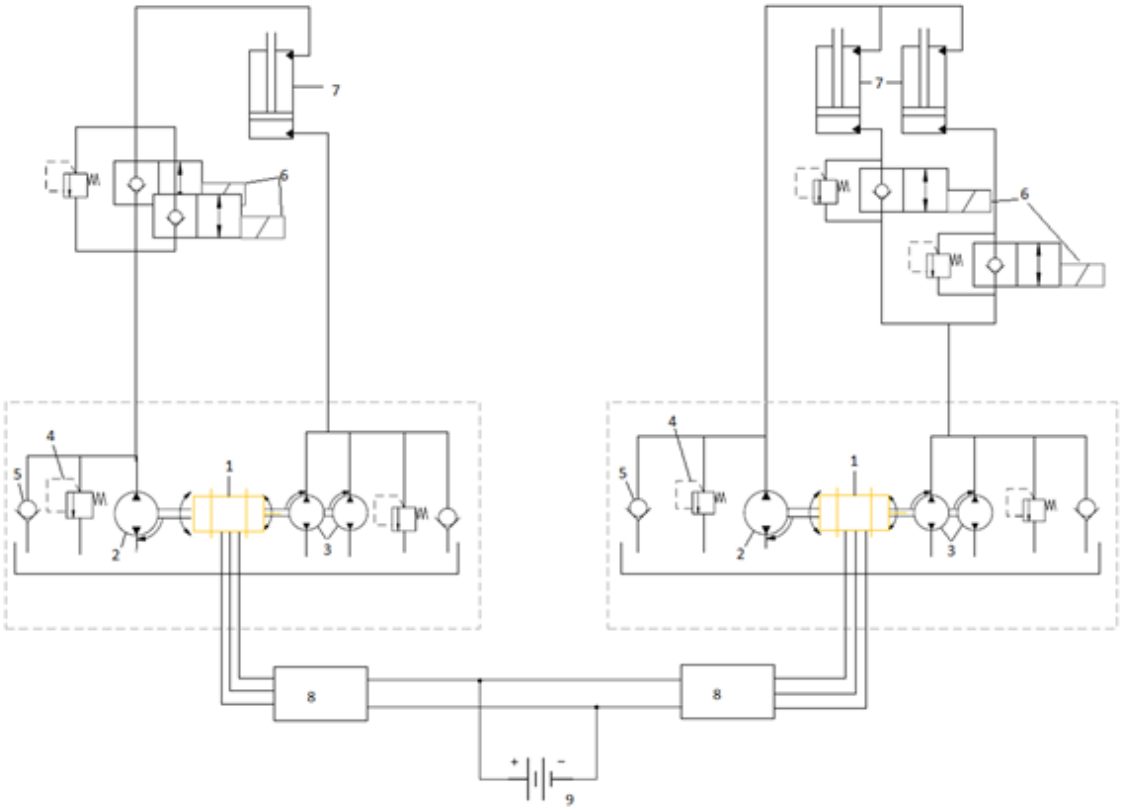

	Component	Model
1	Electric motor	Motenergy ME1304
2	B-side pump	HYDAC PGI100
3	A-side pumps	HYDAC PGI100
4	Pump pressure relief valve	HYDAC DB10P-01
5	Anti-cavitation valve	HYDAC RV12A-01
6	Safety valves	HYDAC WS16ZR-01
7	Hydraulic cylinder	EJC90 original
8	Motor controller	Sevcon Gen 4
9	Lithium-titanate battery	Altairnano 96V

Appendix 2: datasheets of traction motors

SIEMENS

Drive Motor 1PV5138-4WS24

Type	AC Induction Motor
Cooling Media	Water-Glycol
Rated Voltage DC	650 V
Rated Power	85 KW
Rated Torque	220 Nm
Max. Torque	530 Nm @ 300A
Rated Current	142 A
Max. Speed	10,000 rpm
Weight	120 kg
Dim. (LxWxH)	510 x 245 x 245 mm
Ambient Temperature	- 30 °C to 70 °C
Degree of Protection	IP 65 / 9k

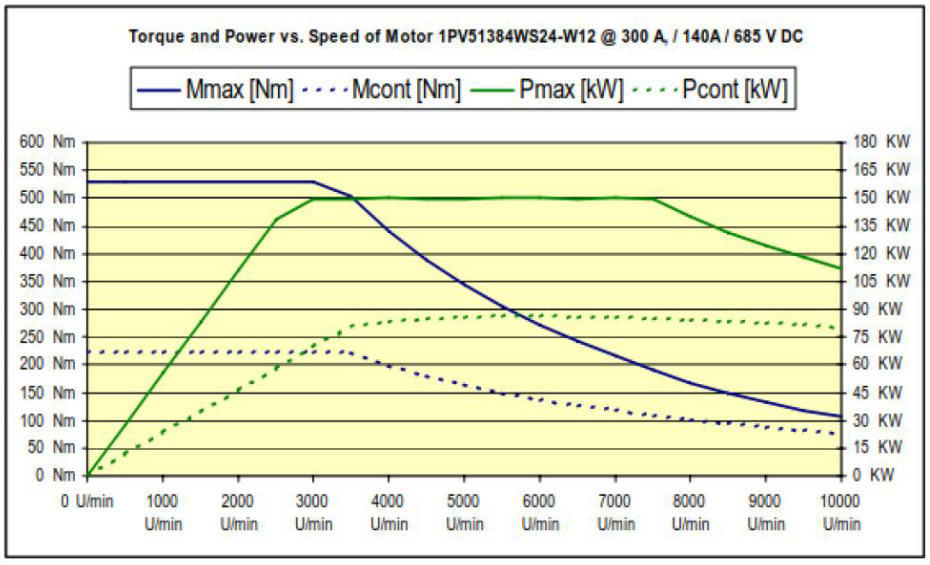

©Siemens ®2011
Industry Sector DT LD T HD, 03/2011

DS_Comp_AM....ppt

The information provided in this brochure contains merely general descriptions or characteristics of performance, which in actual case of use do not always apply as described or which may change as a result of further development of the products. An obligation to provide the respective characteristics shall only exist if expressly agreed in the terms of contract.

SIEMENS

Drive Motor 1PV5135-4WS28

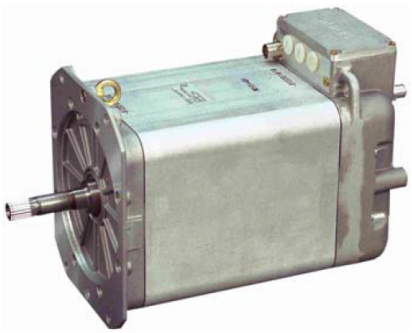

Type	AC Induction Motor
Cooling Media	Water-Glycol
Rated Voltage DC	650 V
Rated Power	67 KW
Rated Torque	160 Nm
Max. Torque	360 Nm @ 250A 430 Nm @ 300A
Rated Current	124 A
Max. Speed	10,000 rpm
Weight	90 kg
Dim. (LxWxH)	425 x 245 x 245 mm
Ambient Temperature	- 30 °C to 70 °C
Degree of Protection	IP 65 / 9k

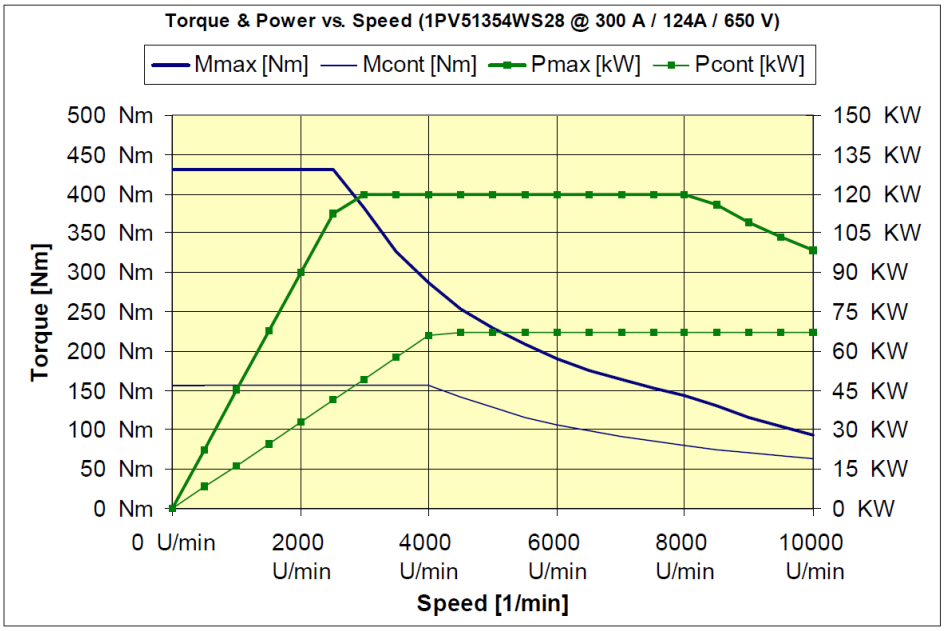

©Siemens ®2011
Industry Sector DT LD T HD, 03/2011

DS_Comp_AM....ppt

The information provided in this brochure contains merely general descriptions or characteristics of performance, which in actual case of use do not always apply as described or which may change as a result of further development of the products. An obligation to provide the respective characteristics shall only exist if expressly agreed in the terms of contract.

Appendix 3: Traction motor efficiency supplied by the manufacturer

n	M	Pmech	ETAmot	ETAumr	ETAges
[min-1]	[Nm]	[kW]	[%]	[%]	[%]
1000	15	1,57	76,5	91	69,6
1000	30	3,14	78	93,1	72,6
1000	45	4,71	78,8	94,1	74,2
1000	60	6,28	79,5	94,7	75,3
1000	75	7,85	79,9	95,1	76
1000	90	9,42	80,5	95,3	76,7
1000	105	11	80,7	95,5	77,1
1000	120	12,57	80,8	95,7	77,3
1000	135	14,14	80,8	95,8	77,4
1000	150	15,71	80,8	95,9	77,4
1000	165	17,28	80,7	95,9	77,5
1000	180	18,85	80,6	96	77,3
1000	195	20,42	80,3	96	77,1
1000	210	21,99	80,2	96	77
1000	225	23,56	79,9	96,1	76,8
1000	240	25,13	79,7	96,1	76,6
1000	255	26,7	79,4	96,1	76,3
1000	270	28,27	79	96,1	75,9
1000	285	29,85	78,8	96,1	75,8
1000	300	31,42	78,5	96,1	75,5
1000	315	32,99	78,2	96,1	75,2
1000	330	34,56	77,9	96,2	74,9
1000	345	36,13	77,7	96,2	74,7
1000	360	37,7	77,4	96,2	74,4
1000	375	39,27	77	96,2	74,1
1000	390	40,84	76,7	96,2	73,7
1000	405	42,41	76,3	96,2	73,4
1000	420	43,98	75,9	96,2	73
1000	435	45,55	75,6	96,2	72,7
1000	450	47,12	75,3	96,2	72,4
1000	465	48,69	74,9	96,2	72,1
2000	15	3,14	80,3	95	76,3
2000	30	6,28	82,8	96,2	79,7
2000	45	9,42	84,4	96,7	81,6
2000	60	12,57	85,6	97,1	83,1
2000	75	15,71	86,4	97,3	84,1
2000	90	18,85	87,1	97,4	84,9
2000	105	21,99	87,6	97,5	85,4
2000	120	25,13	87,9	97,6	85,8
2000	135	28,27	88,1	97,7	86,1
2000	150	31,42	88,3	97,7	86,3
2000	165	34,56	88,3	97,7	86,3
2000	180	37,7	88,3	97,8	86,4
2000	195	40,84	88,3	97,8	86,3
2000	210	43,98	88,2	97,8	86,3
2000	225	47,12	88,1	97,8	86,2
2000	240	50,27	88,1	97,8	86,1
2000	255	53,41	87,9	97,8	86
2000	270	56,55	87,8	97,8	85,9
2000	285	59,69	87,7	97,8	85,8
2000	300	62,83	87,6	97,8	85,7
2000	315	65,97	87,4	97,8	85,5
2000	330	69,12	87,2	97,8	85,4
2000	345	72,26	87	97,8	85,1
2000	360	75,4	86,9	97,8	85
2000	375	78,54	86,7	97,8	84,8
2000	390	81,68	86,5	97,8	84,6
2000	405	84,82	86,3	97,8	84,4
2000	420	87,96	86,1	97,8	84,2
2000	435	91,11	86	97,8	84,1
2000	450	94,25	85,8	97,8	83,9
3000	15	4,71	82,1	96,5	79,2
3000	30	9,42	85,6	97,3	83,3
3000	45	14,14	87,7	97,7	85,7
3000	60	18,85	89,1	97,7	87
3000	75	23,56	90,1	97,9	88,1
3000	90	28,27	90,6	98	88,9
3000	105	32,99	91	98,1	89,3
3000	120	37,7	91,2	98,2	89,6
3000	135	42,41	91,4	98,3	89,8
3000	150	47,12	91,4	98,3	89,8
3000	165	51,84	91,4	98,3	89,9
3000	180	56,55	91,3	98,4	89,8
3000	195	61,26	91,2	98,4	89,7
3000	210	65,97	91,1	98,4	89,7
3000	225	70,69	91	98,4	89,6
3000	240	75,4	90,9	98,4	89,5
3000	255	80,11	90,8	98,4	89,3
3000	270	84,82	90,7	98,4	89,2
3000	285	89,54	90,5	98,4	89,1
3000	300	94,25	90,4	98,4	89
3000	315	98,96	90,3	98,4	88,9
4000	15	6,28	84	97,2	81,6
4000	30	12,57	88,7	97,6	86,6
4000	45	18,85	90,7	98,1	88,9
4000	60	25,13	91,6	98,2	90
4000	75	31,42	92	98,3	90,5
4000	90	37,7	92,2	98,4	90,7
4000	105	43,98	92	98,5	90,6
4000	120	50,27	92,1	98,6	90,8
4000	135	56,55	92,1	98,6	90,8
4000	150	62,83	92,1	98,7	90,8
4000	165	69,12	92	98,7	90,8
4000	180	75,4	92	98,7	90,8
4000	195	81,68	92	98,7	90,8
4000	210	87,96	91,9	98,7	90,7
4000	225	94,25	91,8	98,7	90,6
5000	15	7,85	86,4	97,4	84,2
5000	30	15,71	90,6	98,1	88,9
5000	45	23,56	91,9	98,3	90,4
5000	60	31,42	92,4	98,4	91
5000	75	39,27	92,5	98,5	91,1
5000	90	47,12	92,2	98,7	91
5000	105	54,98	92,4	98,7	91,2
5000	120	62,83	92,5	98,8	91,3
5000	135	70,69	92,5	98,8	91,3
5000	150	78,54	92,4	98,8	91,3
5000	165	86,39	92,3	98,8	91,1
5000	180	94,25	92,1	98,7	91
6000	15	9,42	88,1	97,9	86,2
6000	30	18,85	91,5	98,3	90
6000	45	28,27	92,5	98,5	91,1
6000	60	37,7	92,6	98,6	91,3
6000	75	47,12	92,7	98,7	91,5
6000	90	56,55	92,7	98,8	91,5
6000	105	65,97	92,7	98,8	91,6
6000	120	75,4	92,6	98,8	91,5
6000	135	84,82	92,4	98,8	91,2
6000	150	94,25	92,1	98,7	90,9
7000	15	11	87,9	98,1	86,2
7000	30	21,99	91,4	98,5	90,1
7000	45	32,99	92,5	98,6	91,2
7000	60	43,98	92,6	98,8	91,4
7000	75	54,98	92,7	98,8	91,6
7000	90	65,97	92,7	98,8	91,6
7000	105	76,97	92,5	98,8	91,4
7000	120	87,96	92,1	98,7	90,9
7000	135	98,96	91,5	98,7	90,3
8000	15	12,57	87	98,3	85,5
8000	30	25,13	90,9	98,7	89,7
8000	45	37,7	92,2	98,8	91,1
8000	60	50,27	92,6	98,8	91,5
8000	75	62,83	92,7	98,8	91,6
8000	90	75,4	92,4	98,8	91,3
8000	105	87,96	91,8	98,7	90,6
9000	15	14,14	89,9	98,4	88,5
9000	30	28,27	93,4	98,7	92,1
9000	45	42,41	94,2	98,7	92,9
9000	60	56,55	94,1	98,6	92,8
9000	75	70,69	93,7	98,5	92,3
9000	90	84,82	92,7	98,4	91,2
10000	15	15,71	90,3	98,6	89
10000	30	31,42	93,5	98,7	92,3
10000	45	47,12	94,1	98,6	92,8
10000	60	62,83	93,7	98,5	92,4
10000	75	78,54	92,8	98,4	91,3

Appendix 4.1: Cycle1.m

```
% Defines the work cycle for them mining loader

clear
B=150;                                          % length of cycle in seconds
t = [0:1:B]';                                   % time vector
A(1:B/2-10)=5;                                  % maximum reference speed
speed = [0 1 2 3 4 A 4 3 2 1 0 ...
0 1 2 3 4 A 4 3 2 1 0 0]';                      % speed reference as constant
acceleration and constant speed

spd_min = speed*0.5;                            % minimum speed limit
spd_max = speed*2;                              % maximum speed limit
distance = cumtrapz(t,speed);                   % distance as an integration
of speed function

distance_diff = diff(distance);
distance_diff = [0; distance_diff];             % change in distance at every
second

slope = zeros(length(t),1);
slope(1:floor(B/8),1) = 0.07;
slope(floor(B/8+1):floor(3*B/8),1) = -0.209;
slope(floor(5*B/8+1):floor(7*B/8),1) = 0.209;
slope(floor(7*B/8+1):ceil(B)+1,1) = -0.07;      % slope at every second of
the cycle

veh_data.time_ref=t;
veh_data.dist_ref=distance_diff;
veh_data.spd_ref=speed;
veh_data.spd_lim=[spd_min spd_max];
veh_data.slope_ref=slope;                       % flushing work cycle data
to data file

load('Eff_map');
tmp.etam = [Efficiencymap/100];                 % load motor efficiency map
```

Appendix 4.2: DP_data.m

```
% Defines vehicle parameters for mining loader

%=========================================================================
==
% Vehicle data
%=========================================================================
==

% General vehicle data
veh_data.wh_radius = 0.62;           % wheel radius
veh_data.wh_inertia = 10;            % wheel inertia
veh_data.veh_air_density = 1.23;     % air density
veh_data.veh_FA = 6.2;               % vehicle frontal area
veh_data.veh_CD = 0;                 % drag coefficient
veh_data.veh_mass = 14000;           % vehicle mass
veh_data.load = 4000;                % mined rock load
veh_data.veh_gravity = 9.8066;       % g
veh_data.wh_1st_rrc = 0.01;          % rolling resistance
veh_data.amb_tmp = 25;               % ambient temperature
veh_data.acc_pwr = 10000;            % constant auxiliary power

% Transmission data.
veh_data.fd_ratio = 1*5.125*6;       % final drive gear ratio 1;2.2;4.39
veh_data.gb_eff = 0.98;             % efficiency, includes final drive and
axle

% Electric motor data
veh_data.mc_inertia = 0.094;         % motor inertia
veh_data.mc_gear_ratio = 2;          % motor gear ratio

% motor speed list (rad/s)
veh_data.wm_list = [0 1000   2000    3000   4000   5000   ...
    6000   7000   8000   9000 10000]/60*6.28;
% motor torque list (Nm)
veh_data.Tm_list = [0 15 30 45 60 75 90 105 120 135 ...
    150 165 180 195 210 225 240 255 270 285 300 315 330 345 ...
    360 375 390 405 420 435 450 465];
% motor maximum torque (Nm) 2 motors
veh_data.Tmmax   = [465 465   465   315   225   180   150   ...
    135   105   90   75]*2;
% motor minimum torque (indexed by speed list)
veh_data.Tmmin   = -veh_data.Tmmax;
% motor efficiency map (indexed by speed list and torque list)
veh_data.etam = tmp.etam';

% Battery data
veh_data.batt_ah = 40;               % battery capacity
veh_data.batt_nom_dis_c = 200;       % nominal discharging current
veh_data.batt_max_dis_c = 400;       % maximum discharging current
veh_data.batt_max_chg_c = 80;        % maximum charging current
veh_data.batt_mods = 17*6;           % battery modules, 1 battery was not
powerful enough
```

```
veh_data.batt_packs = 1;              % battery packs
veh_data.batt_mod_mass = 7.7;         % battery module mass
veh_data.batt_mod_cp = 750;          % J/kgK average heat capacity of module
veh_data.batt_th_res = 0.20;          % K/W module thermal resistance
veh_data.batt_mod_airflow = 0.03;     % kg/s cooling air mass flow rate
across module

% state-of-charge list
veh_data.soc_list = 0:0.1:1;
% open circuit voltage (indexed by state-of-charge list)
veh_data.V_oc = [24.2 24.2 24.2 24.2 24.2 24.2 24.2 24.2 24.2 24.2
24.2]*veh_data.batt_mods;
% discharging resistance (indexed by state-of-charge list)
veh_data.R_dis = ones(size(veh_data.soc_list))*0.0175*veh_data.batt_mods;
% charging resistance (indexed by state-of-charge list)
veh_data.R_chg = veh_data.R_dis;
% battery initial state of charge
veh_data.init_soc = 0.8;


% Post processing excluded
```

Appendix 4.3: RunDP_loader.m

```
% Runs dynamic programming optimization for mining loader

tic
plot_on = 1;

%=========================================================================
==
% Initialization
%=========================================================================
==

% vehicle data
veh_data.veh_file = 'DP_data';
eval(veh_data.veh_file)
%%
%=========================================================================
==
% DP initialization data
%=========================================================================
==

    t_step = 0.5;   % Default value 0.5, higher values produce inaccurate
results!
    fprintf('\n');
    disp(['Time grid: ' num2str(t_step)])

%=========================================================================
==
% create grid
%=========================================================================
==
    c=2;                                              % 2 cycles, one with
load and one without
for i_k = 1:c
    % set initial state
    cyc_time = veh_data.time_ref(end)/c;             % length of the cycle
    grd.Xn{1}.hi = cyc_time*1.02;                     % upper boundary of
the state grid
    grd.Nx{1} = ceil(grd.Xn{1}.hi/t_step/10)*10;     % number of elements
in the state grid
    grd.Xn{1}.lo = 0;                                % minimum value of the
time range of the subcycle.
    grd.Nu{1}    = grd.Nx{1};                         % number of elements
in the input grid
    grd.Un{1}.hi = 1;                                 % upper boundary of
the input grid (always 1)
    grd.Un{1}.lo = 0;                                 % lower boundary of
the input grid (always 0)
    grd.X0{1} = 0;                                   % initial state
    grd.XN{1}.hi = cyc_time*1.5;                      % final state upper
constraint
    grd.XN{1}.lo = cyc_time/1.5;                      % final state lower
constraint
```

```
%=========================================================================
==
% Speed
%=========================================================================
==

    grd.Nx{2}    = grd.Nx{1};  % same size as state grid
    grd.Xn{2}.hi = 10;         % Maximum allowed speed.
    grd.Xn{2}.lo = 0;          % Minimum allowed speed.
    grd.Nu{2}    = 1;          % This is the second control par, unused.
    grd.Un{2}.hi = 5;
    grd.Un{2}.lo = 0;
    grd.X0{2} = 0;       % Initial speed.
    grd.XN{2}.hi = 0;    % Maximum allowed speed at the end of the cycle.
    grd.XN{2}.lo = 0;    % Minimum allowed speed at the end of the cycle.

%=========================================================================
==
% Problem definition (definition of the cycle)
%=========================================================================
==
    % cycle precision
    veh_data.cyc_dt = 1;

    if i_k==1
        start = 1;                                % Start time of the cycle.
        stop = ceil(size(veh_data.time_ref,1)/c);% End time of the cycle.
    else
        start = ceil(size(veh_data.time_ref,1)/c)+1;
        stop = ceil(size(veh_data.time_ref,1));
    end
    % reference speed
    prb.W{1} = veh_data.spd_ref(start:veh_data.cyc_dt:stop,1);
    % minimum speed
    prb.W{2} = veh_data.spd_lim(start:veh_data.cyc_dt:stop,1);
    % maximum speed
    prb.W{3} = veh_data.spd_lim(start:veh_data.cyc_dt:stop,2);
    % distance
    prb.W{4}                                                                  =
veh_data.dist_ref(start:veh_data.cyc_dt:stop,1)*veh_data.cyc_dt;
    % elevation,
    prb.W{5} = veh_data.slope_ref(start:veh_data.cyc_dt:stop,1);

    % step size
    prb.Ts = 1;                           % time step
    prb.N  = length(prb.W{1})*1/prb.Ts; % number of time steps in problem
(defines the problem length)

    % DP options
    options = dpm();                      % load dpm options structure
    options.BoundaryMethod = 'none';     % Tai BoundaryMethod
    options.SaveMap = 1;                  % on/off to save cost-to-go map
    options.MyInf = 1000;                % a big number for infeaible states
(where I=1)
    options.Iter = 5;                        % maximum number of iterations
when inverting model
    options.InputType = 'c';             % c -continuous input, d - discreet
```

```
    options.FixedGrid = 0;              % defined or adjustable grid
    options.Minimize = 1;               % 1 - minimizing 0 - maximizing

    % dynamic programming solver
    [res, dyn] = dpm(@DP_model,veh_data,grd,prb,options); % runs dpm
backwards with given model
    [res_fwd] = DP_run_fwd(prb, veh_data);                % runs forward
with optimal policy
```

Appendix 4.4: DP_model.m

```
function [X, C, I, out] = DP_model(inp,par)
%=========================================================================
==
% VEHICLE
%=========================================================================
==
%%
    spd = inp.U{1}.*(inp.W{3}-inp.W{2})+inp.W{2}; % vehicle speed

    %redefine variables
    dt = inp.W{4}./spd;                             % W{4} is distance
    dt(~isfinite(dt)) = 0;
    X{1} = dt+inp.X{1};                             % time
    X{2} = spd;                                     % speed

    acc = (X{2}-inp.X{2})./dt;                      % vehicle acceleration
    acc(~isfinite(acc)) = 0;
    ina = (acc > 3) + (acc < -3);                       % define infeasible
acceleration

    wv  = spd ./ par.wh_radius;                     % Wheel speed (rad/s)
    dwv = acc ./ par.wh_radius;                        % Wheel acceleration
(rad/s^2)
    Tw0 = 0;                                        % Wheel drag torque

    % Wheel torque (Nm)
    Tv = (0.5*par.veh_air_density*par.veh_FA*par.veh_CD*spd.^2+ ...

par.veh_mass*par.veh_gravity*par.wh_1st_rrc*cos(inp.W{5})+par.veh_mass*ac
c+ ...
    par.veh_mass*par.veh_gravity*sin(inp.W{5})).*par.wh_radius+Tw0;     %
inp.W{5} is road inclination (rise per distance).

%=========================================================================
==
% MOTOR
%=========================================================================
==
%%
% Electric motor speed (rad/s)
mwg  = par.fd_ratio*par.mc_gear_ratio .* wv;

% Electric motor acceleration (rad/s^2)
dwg = par.fd_ratio*par.mc_gear_ratio .* dwv;

% Electric motor drag torque (Nm)
Tm0 = par.mc_inertia.*dwg; %

% Electric motor torque (Nm)
Tm  = (Tv>0)  .* Tv ./ par.mc_gear_ratio ./ par.fd_ratio ./ par.gb_eff...
    + (Tv<=0) .* Tv ./ par.mc_gear_ratio ./ par.fd_ratio .* par.gb_eff +
Tm0;

% Electric motor efficiency
```

```
e_mc                    =                    (mwg~=0)                    .*
interp2(par.Tm_list,par.wm_list,par.etam,abs(Tm),mwg.*ones(size(Tm)))    +
(mwg==0);

% Summarize infeasible, only this causes infeasible solutions.
inm     =     (isnan(e_mc))     +     (Tm<0)          .*     (Tm     <
interp1(par.wm_list,par.Tmmin,mwg,'linear*','extrap')) +...
                       (Tm>=0)             .*             (Tm             >
interp1(par.wm_list,par.Tmmax,mwg,'linear*','extrap'));

% Calculate electric power consumption
Pm =  (Tm<0) .* mwg.*Tm.*e_mc + (Tm>=0) .* mwg.*Tm./e_mc;

% Total required power (W)
Ptot = Pm+par.acc_pwr;
Pbe  = Ptot;
%=========================================================================
==
% BATTERY
%=========================================================================
==
%%
% Battery efficiency
e = (Pbe>0) + (Pbe<=0) .* 0.98; % % coulumbic efficiency (0.98 when
charging)

% Battery internal resistance
r     =     (Pbe>0)          .*     interp1(par.soc_list,     par.R_dis,
0.8,'linear*','extrap')...
  + (Pbe<=0) .* interp1(par.soc_list, par.R_chg, 0.8,'linear*','extrap');
% SOC constant 0.8 (or 80%). (This line calculates battery resistance.)

% Battery current limits
im  =  (Pbe>0)  .*  par.batt_max_dis_c*par.batt_packs  +  (Pbe<=0)  .*
par.batt_max_chg_c*par.batt_packs;

% Battery voltage
v = interp1(par.soc_list, par.V_oc, 0.8,'linear*','extrap');

% Battery current
Ib  =   e .* (v-sqrt(v.^2 - 4.*r.*Pbe))./(2.*r);

% Battery power consumption
Pb = Ib .* v;
% Battery loss power
P_loss = abs(Pb-Pbe); %r.*Ib.^2;
% Efficiency
e_bt = abs(Pb)./(abs(Pb)+P_loss); %not used
% Power cost
Pcost = abs(Pb-Tm.*mwg)/1e6;%(Pb./(1./spd))/3.6e6;%
% Update infeasible
inb = ((v.^2 < 4.*r.*Pbe) + (abs(Ib)>im));

% Set new state of charge to real values
X{1} = (conj(X{1})+X{1})/2;
X{2} = (conj(X{2})+X{2})/2;
Pb   = (conj(Pb)+Pb)/2;
```

```
Ib    = (conj(Ib)+Ib)/2;


% COST
% Summarize infeasible matrix
I = (ina+inb+inm~=0);

% Calculate cost matrix (energy losses)
C{1} =Pb/1e6+acc;

% store relevant signals in out [excluded]
% DPM and forward simulation excluded
```